People's Democratic Republic of Algeria
Ministry of Higher Education and Scientific Research

UNIVERSITY OF SAAD DAHLEB BLIDA

Institution of Aeronautics and Spatial Studies (IASS)

Thesis for obtaining the Master's degree in Aeronautics

Option: Aircraft Propulsion

Theme:

SIMULATION OFTURBULENT PREMIXED METHANE/AIR COMBUSTION USING OPENFOAM

Framed by:

Dr. NECHE Ahmed (IASS)

Dr. RENANE Rachid (IASS)

Realized by:

Mr. BOULEGHLEM Houssem Eddine

2023/2024

Abstract:

In this study, we simulated the turbulent premixed combustion of a methane/air mixture using the open-source computational fluid dynamics (CFD) software OPENFOAM. The mathematical model employed is based on solving the Navier-Stokes (NS) equations with turbulence modeled using the RANS (k-epsilon realizable) approach. We examined a detailed chemical mechanism comprising 41 reactions for two equivalence ratios ($\varphi = 0.56$ and $\varphi = 0.43$) derived from published experimental data, with the mixture preheated to 673 K, at a pressure of 5 bars, and a jet velocity of 40 m/s.

The results show a better match with the published experimentally measured flame length for an equivalence ratio of $\varphi = 0.43$, suggesting that the model is adequate when finite rate effects are dominant. However, it requires adjustments for flames closer to the flamelet regime.

Résumé :

Dans cette étude, nous avons simulé la combustion prémélangée turbulente du mélange méthane/air à l'aide du logiciel open-source de dynamique des fluides computationnelle (CFD) OPENFOAM. Le modèle mathématique utilisé est basé sur la résolution des équations de Navier-Stokes (NS) avec la turbulence modélisée par l'approche RANS (k-epsilon réalisable). Nous avons examiné un mécanisme chimique détaillé comportant 41 réactions pour deux rapports d'équivalence ($\varphi = 0{,}56$ et $\varphi = 0{,}43$) dérivés de données expérimentales publiés, avec un mélange préchauffé à 673 K, une pression de 5 bars et une vitesse de jet de 40 m/s.

Les résultats montrent une meilleure correspondance avec la longueur de flamme mesurée expérimentalement pour une richesse de $\varphi = 0{,}43$, ce qui suggère que le modèle est adéquat lorsque les effets de taux finis sont dominants. Cependant, il nécessite des ajustements pour les flammes plus proches du régime de flamelet.

ملخص:

في هذه الدراسة، نهدف إلى محاكاة تأثير نسبة المعادلة على احتراق الميثان التوربيني باستخدام برنامج حساب ديناميك السوائل "أوبن فوم ".

على الرغم من أن النمذجة السابقة لهذه التجارب تركزت على طرق الكيمياء المبنية على الجداول المسبقة، إلا أننا في هذا العمل نبحث في الكيمياء العامة (ميكانيكية تفاعلية تحتوي على 41 تفاعلًا) ($\varphi = 0.43$ و$\varphi = 0.56$) باستخدام نموذج "ريلايزابل كاي ابسيلون". ثم اختيار نسبتين معادلة تتوافق مع أقصى طول للشعلة من قاعدة البيانات التجريبية.

التسخين المسبق للخليط عند 673 كلفن، وضغط 5 بار، وسرعة تدفق 40 م/ث. تم تحقيق تطابق أفضل مع بيانات طول الشعلة المقاس تجريبيًا المنشورة لنسبة المعادلة 0.43 من نسبة المعادلة 0.56، مما يشير إلى أن النموذج مناسب عندما تكون تأثيرات معدل الانتشار مهيمنة ولكنه يتطلب توسيعًا للشعلات الأقرب إلى نظام الشعلة الانسيابي.

Acknowledgments

If it takes a lot of motivation, rigor, and enthusiasm to successfully complete this thesis, then at First I thank God, that gives strength and will, and that subjected to me people to assist me and help build my career.

This research work needed the contribution of several people, whom I would like to thank: my supervisors, Mr A.NECHE& Mr R. RENANE, for all their valuable advices, for their active listening, their availability and guidance.

Indeed, I obviously express all my gratitude to all my teachers at the Institute of Aeronautics and Space Studies for the knowledge they have imparted to me during my five years of study.

My thanks also go to the members of the jury who honor me by evaluating this modest work. To my parents, brothers, family and loved ones, who supported me during moments of doubt and abandonment, who believed in me.

I hope that I will use my knowledge and strength to benefit my country and all the people that I shape a bond with.

Table of Contents

List of Figures

List of Tables:

List of Symbols

CFD	Computational Fluid Dynamics
RANS	Reynolds Average Navier Stockes
φ,Ø	Equivalence ratio
LPC	Lean Premixed Combustion
CNG	Compressed Natural Gas
Y(k)	Mass Fraction of Specie k
Mk	Molar Mass of Specie k
Re	Reynolds Number
u(t)	Instantaneous Velocity
U	Average Velocity
u'(t)	Fluctuating Velocity

Urms,RMS	Velocity Root Mean Squared
k	Turbulent Kinetic Energy
LTS	Local Time Stepping
PIMPLE	Combination of PISO and SIMPLE Algorithms
PISO	Pressure Implicit with Splitting of Operator
SIMPLE	Semi-Implicit Method for Pressure-Linked Equations
h	enthalpy
T	Temperature
P	pressure
U	Velocity
ρ	Density
μ	Dynamic Viscosity
Cp	Calorific Capacity
k(A)	Reaction Rate of Specie A
Ea	Activation Energy
R	gas constant
A	pre- exponential factor
M	Collision Partner
τ*	Finite Reaction Time Scale
qr	Radiation Heat Release
D	Inlet Cylinder Diameter
r	Radial Distance from Centerline
U norm	Normalized Axial Velocity
RMS norm	Normalized RMS
μ	Dynamic viscosity
κ	EDC Coefficient

Introduction

Recently, there has been a significant increase in fundamental research driven by growing environmental concerns. These concerns are mainly related to reducing emissions and improving control of combustion devices, specifically aiming for better flame stability in gas turbines. As a result, environmental laws on emissions (CO2, NOx, CO) have become more stringent. These restrictions have put pressure on advanced combustion technologies like lean premixed combustion, highlighting the need to maximize the potential of these techniques. To achieve this, detailed fundamental research is necessary, made possible by significant advancements in experimental techniques, such as laser spectroscopy.

The focus of this Master's work is on the combustion of methane, which is the primary component of natural gas commonly used to power stationary gas turbines.

Gas turbines play a significant role in energy production, contributing to a substantial share of the global energy output. For instance, in 2002, natural gas-powered gas turbines accounted for approximately 17% of the total electricity produced worldwide. This share is expected to grow in the future due to several advantages of natural gas combustion, including the ability to achieve very low NOx emissions.

Currently, lean, premixed combustion (LPC) is a well-established technology used in stationary gas turbines powered by natural gas. It allows for low emissions while maintaining high efficiency. It is believed that a better understanding of the turbulence-chemistry interactions will lead to improvements in the combustion process. This understanding is important for both practical applications, such as gas turbine combustors, and fundamental research.

During the 30th International Symposium on Combustion, R.W. Bilger emphasized in a comprehensive anniversary lecture that the complexity of turbulence-chemistry interactions in premixed flames has not been adequately explored. It remains one of the biggest challenges in combustion research. Specifically, characterizing turbulent lean premixed flames under typical gas turbine operating conditions has not reached a satisfactory level. Although there are numerous studies on turbulent premixed flames in the literature, data on gas turbine relevant conditions is scarce.

The focus of this work is twofold:

Firstly, it aims to comprehensively characterize turbulent premixed flames under conditions typical for gas turbines, including high pressure and elevated temperatures, fuel-lean environments, and intense turbulence.

Secondly, this research aims to serve as a reference for future combustion simulations using OPENFOAM, which has emerged as the leading open-source CFD software in recent years.

The investigation will explore the influence of operating conditions, such as fuel concentration and preheating temperature, on the position, shape, and fluctuations of the flamefront.

The primary objective of this work is to pave the way for students to utilize OPENFOAM software in studying complex topics such as the interaction between turbulence and chemistry in turbulent premixed flames under relevant operating conditions

This work is divided into the following chapters:

Chapter 1: "Generalities" introduces the essential concepts of methane combustion, focusing on its industrial importance and applications. It explains the difference between premixed and non-premixed combustion, covers the chemical properties of methane, the stoichiometry of combustion reactions, and the concept of equivalence ratio. The chapter also explores the nature of turbulence and its effects on flame propagation, providing some basic information about turbulence.

Chapter 2: "Turbulent Combustion Modeling Using OpenFOAM" delves into the techniques and methodologies for simulating turbulent combustion using the OpenFOAM software. It begins with an introduction to OpenFOAM, an open-source computational fluid dynamics (CFD) toolbox, and its relevance in combustion modeling. The chapter explains the basics of setting up a turbulent combustion simulation, including the numerical equations, turbulence models, combustion models, and the integration of chemical kinetics and thermodynamic properties in the simulation process.

Chapter 3: "Case Setup" provides a comprehensive guide to setting up simulations for

turbulent combustion using OpenFOAM. It starts with an overview of the essential components of a case setup, including geometry and mesh generation and refinement. The chapter concludes with best practices for monitoring simulation progress, analyzing results, and ensuring the validity and accuracy of the simulation setup.

Chapter 4: "Results and Discussion" focuses on the analysis and interpretation of simulation outcomes for turbulent combustion using OpenFOAM. It begins by outlining the key metrics and parameters to evaluate, such as temperature distribution, using ParaView for graphical representation of results. The chapter includes guidelines for comparing simulation results with published experimental data or validating the model. The discussion section addresses the implications of the findings, highlighting trends, anomalies, and the influence of various parameters on combustion behavior. Finally, the chapter suggests improvements for future simulations and concludes with a summary of key insights gained from the simulations and their relevance to real-world turbulent combustion applications.

Finally, this work concludes with a summary of our findings, followed by potential outlooks for future research in this area.

CHAPTER.1: Generalities

1.1. State of the Art:

Historical Background Methane's presence and importance have been recognized since ancient times, with its first scientific documentation dating back to Alessandro Volta in the 18th century. It was identified as a discrete substance in marsh gas, leading to its name derived from 'methy' meaning wine and 'hydor' meaning water. Methane's role as a fuel became prominent with the advent of industrialization, where it was harnessed for lighting and heating.

Usage as Fuel Methane's versatility as a fuel is evident in its widespread use across various sectors. In households, it powers heating systems and cooking appliances. Industrially, it fuels kilns and turbines and is integral to electricity generation through gas turbines or steam generators. The transportation sector also benefits from methane as a clean alternative to traditional fossil fuels, powering vehicles with compressed natural gas (CNG) engines.

Modern Research The 21st century has seen a surge in research aimed at optimizing methane combustion for energy production with minimal environmental impact. Key areas of focus include the development of low-temperature combustion techniques, advanced oxidation mechanisms, and novel catalysts that facilitate more efficient methane combustion processes. The "Two-term" model has been instrumental in understanding the complex kinetics involved in methane oxidation, paving the way for catalysts that can operate effectively at lower temperatures and pressures.

The article titled **"Experimental and Theoretical Study of Diffusion Combustion of Methane" by** Donskoy, I.G., Misyura, S.Y focuses on the stability of methane hydrate combustion, determined by the heat release and transfer ratio. It includes experiments on methane combustion above a dissociating gas hydrate layer and proposes a mathematical model for estimating diffusion combustion stability.

In a publication by N. I. Gurakov, O. V. Kolomzarov, D. V. Idrisov, S. S. Novichkova, L. Sh. Emirova, V. Yu. Abrashkin, S. S. Matveev, S. G. Matveev, N. I. Fokin, N. O. Simin, A. A. Ivanovskii & D. S. Tarasov titled **"Numerical and Experimental Study of Combustion of Methane–Hydrogen Mixtures"** involves both numerical and experimental analysis of combustion product concentrations and pollutant emissions when burning premixed methane–hydrogen mixtures in a model gas-turbine power plant combustion chamber.

On the article **"Recent Advances in Catalysts for Methane Combustion"** written by Jinghuan Chen, Hamidreza Arandiyan, Xiang Ga & Junhua Li the article reviews publications related to the combustion of methane, focusing on the number of publications from the top 15 publishing nations on the topic of methane catalytic combustion.

Another Previous work done by Niklas Zettervall , Christer Fureby and Elna J. K. Nilsson titled: **"Evaluation of Chemical Kinetic Mechanisms for Methane Combustion: A Review"** the work studies the importance of methane as a fuel for gas turbines, engines, and fundamental combustion studies is highlighted. The paper emphasizes the significance of chemical kinetic mechanisms for methane combustion in Computational Fluid Dynamics (CFD) modeling.

The Article "**Methane Combustion Kinetics over Palladium-Based Catalysts: Review and Perspectives**" done by Roshni Sajiv Kumar, Joe P Mmbaga , Natalia Semagina and R. E. Hayes review discusses kinetic models for precious metal catalysts used in catalytic combustion of lean methane mixtures, providing insights into the current state of the art.

In the publication titled **"LOX/Methane In-Space Propulsion Systems Technology Status and Gaps"** by Klem, Mark D. The paper covers over 50 years of research efforts into methane propulsion, from fundamental combustion and mixing studies to rocket chamber and system-level demonstrations.

Future Prospects Looking ahead, methane's role in sustainable energy production is set to expand. Innovations such as methane-based rocket fuel are being explored for space exploration applications. On Earth, advancements in catalytic technologies are transforming methane into a cornerstone for future organic chemistry and energy systems. Methane fuel cells represent a frontier in energy conversion, potentially revolutionizing how we generate electricity while curbing greenhouse gas emissions.

This expanded overview delves deeper into the historical evolution, current research endeavors, practical uses, and forward-looking perspectives on methane in the context of turbulent combustion.

1.2. Combustion Generalities:

Combustion is a chemical reaction that occurs when oxygen from the air combines with a fuel and a source of heat. Combustion is a reaction that releases heat (exothermic reaction). It occurs either in an 'open' system or in a 'closed' system (in other words, without the exchange of heat and matter with the external environment). Overall, it is a chemical reaction that only takes place when chemical species interact with each other or are close enough to mutually alter each other. Combustion is also an oxidation reaction of combustible material by oxygen (oxidizer), and the products of this reaction are called smoke or unburned residues.

Figure 1. 5 The Fire Triangle

1.2.1. Types of Combustion

There are primarily three types of combustion:

1. **Complete Combustion**: This occurs when a fuel burns in sufficient oxygen, producing a limited number of by-products. These are typically carbon dioxide (CO2) and water vapor (H2O). This type of combustion releases the maximum amount of energy.

2. **Incomplete Combustion**: When the supply of oxygen is limited, incomplete combustion occurs. This results in the production of carbon monoxide (CO), water vapor, and sometimes even carbon soot or carbon particles.

1.2.2. Modes of Combustion

The modes of combustion are categorized based on the propagation of the combustion zone:

1. **Deflagration**: In this mode, the combustion wave propagates at a velocity less than the speed of sound in the non reacted medium.
2. **Detonation**: Here, the combustion wave propagates at a velocity greater than the speed of sound (supersonic).

1.2.3. Varieties of Combustion

- **Premixed Combustion**: The fuel and oxidizer are mixed before combustion. An example is the combustion in a gas stove.

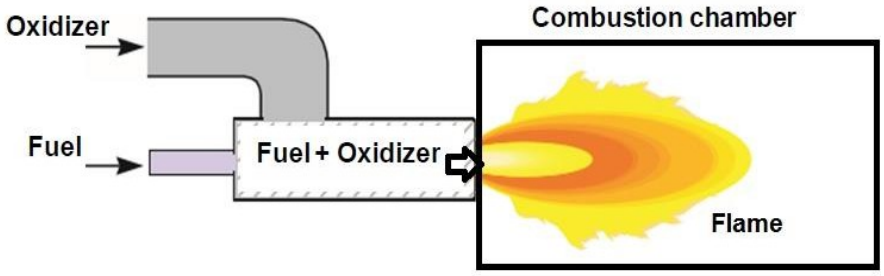

figure 1. 6 Premixed Combustion

- **Non-premixed Combustion**: The fuel and oxidizer are not mixed until they reach the combustion zone. An example is the combustion in a diesel engine.

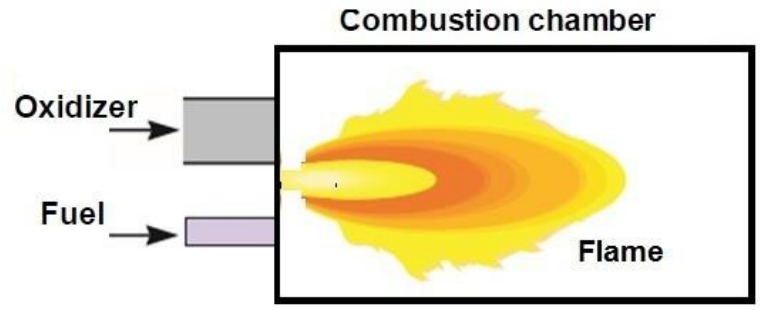

Figure 1. 7 Non Premixed Combustion

1.3. Methane:

Methane is a chemical compound with the chemical formula CH4, discovered and isolated by Alessandro Volta between 1776 and 1778. It is the simplest hydrocarbon and the first term in the family of alkenes. Under normal temperature and pressure conditions, methane is a colorless and odorless gas. About twice as light as air, it is explosive in a confined environment (firedamp). In an unconfined environment, it dilutes in the air and escapes towards the upper atmosphere, where it is less likely to form explosive clouds than gases heavier than air (propane, butane); however, it is a greenhouse gas. Methane is a fuel that makes up to 90% of natural gas. Its auto-ignition temperature in the air is 540°C. Chemical formula of methane:

CH4 Molar mass: 16.04 g/mol; C=74.87%, H=25.13%

1.4. Technologies and Applications:

1. **Space Exploration**: Methane-powered engine components are being tested for next-generation landers. Methane is a promising fuel for the journey to Mars because it's more stable than liquid hydrogen, today's most common rocket fuel, and can be stored at more manageable temperatures.
2. **Fuel Cells**: Methane-based fuel cells are an alternative to hydrogen fuel cells that utilize hydrocarbons to generate electricity. These fuel cells are appealing due to the ready availability of hydrocarbons, both as anthropogenic pollutants from sources such as landfills, and as byproducts of fossil fuel power generation.
3. **Domestic Use**: Methane is used as a fuel for ovens, homes, water heaters, kilns, automobiles, turbines, etc. As the major constituent of natural gas, methane is important for electricity generation by burning it as a fuel in a gas turbine or steam generator.
4. **Industrial Use**: Methane is a critical source of heat and power for various industries, including metals, cement, and glass manufacturing.
5. **Transportation**: Compressed natural gas (CNG), predominantly methane, is used as a cleaner alternative to gasoline and diesel in vehicles.

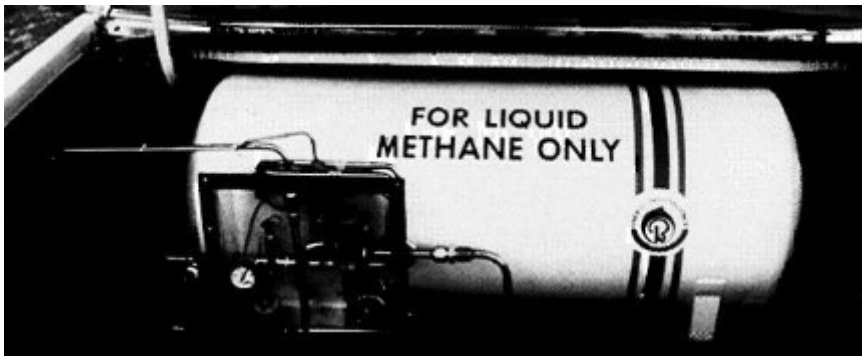

Figure 1. 8 fuel tank of a methane power vehicle (1)

6. **Chemical Industry**: Methane reacts with steam at high temperatures to yield carbon monoxide and hydrogen; the latter is used in the manufacture of ammonia for fertilizers and explosives. Other valuable chemicals derived from methane include methanol, chloroform, carbon tetrachloride, and nitro methane.

1.5. Equivalence Ratio Chemistry and Mass Fractions:

The equivalence ratio (φ) in combustion chemistry is a measure of the ratio of the actual fuel-to-oxidizer ratio to the stoichiometric fuel-to-oxidizer ratio. It's a crucial parameter in analyzing combustion processes, particularly in determining whether a mixture is lean or rich.

Mathematically, it can be defined as:

$$\emptyset = \frac{\left(\frac{fuel}{Air}\right)_{mixture}}{\left(\frac{Fuel}{Air}\right)_{stoichiometric}} \qquad \mathbf{1.1}$$

If $\emptyset > 1$, the mixture is fuel-rich (more fuel than needed for complete combustion).
If $\emptyset < 1$, the mixture is fuel-lean (less fuel than needed for complete combustion).
If $\emptyset = 1$, the mixture is stoichiometric (just enough fuel for complete combustion).
Example: Let's consider the combustion of methane (CH_4) with air (which is approximately 21% O_2 and 79% N_2 by volume) as an example. The stoichiometric reaction is:

$$\mathbf{CH_4 + 2O_2 + 7.52N_2 \rightarrow CO_2 + 2H_2O + 7.52N_2}$$

M(CH_4): 1C + 4H = 12.01 g/mol + 4(1.008 g/mol) = 16.04 g/mol

M(O_2): 2O = 2(16.00 g/mol) = 32.00 g/mol

M(N_2): 2N = 2(14.01 g/mol) = 28.02 g/mol

Mass Fractions:

$$\boldsymbol{Y(k) = \frac{\sum_{i=1}^{k} n_k \cdot M_k}{\sum_{i=1}^{n} n_i \cdot M_i}} \qquad \mathbf{1.2}$$

Where:

k:known specie.

Y(k): mass fraction of specie k.

n_k: moles of specie k

M_k: Molar Mass of specie k

Mass fraction of stoichiometric reaction $\emptyset = 1$

Next, we calculate the total mass of the reactants in the stoichiometric reaction:

- n M(Ch4)=: 1 mol × 16.04 g/mol = 16.04 g
- n M(O2): 2 mol × 32.00 g/mol = 64.00 g
- n M(M2): 7.52 mol × 28.02 g/mol = 210.63 g

Finally, we calculate the mass fraction of each reactant:

- $Y(CH4) = 16.04\ g\ /\ 290.67\ g = 0.055\ or\ 5.5\%$
- $Y(O2) = 64.00\ g\ /\ 290.67\ g = 0.220\ or\ 22.0\%$
- $Y(N2) = 210.63\ g\ /\ 290.67\ g = 0.724\ or\ 72.4\%$

So, in the stoichiometric combustion of methane, the mass fractions of methane, oxygen, and nitrogen are approximately 5.5%, 22.0%, and 72.4%, respectively.

In this example on this paper, we evaluate two values of

Table 1.1 Mass fractions of reactors in methane combustion for different equivalence ratios

	CH4	O2	N2
Stoichiometric $\emptyset = 1$	0.055	0.22	0.724
Poor $\emptyset = 0.56$	0.031603	0.225734	0.742663

Poor $\emptyset = 0.43$	0.024446	0.227402	0.748152

1.6. Turbulence

Turbulent flows are encountered in many technical devices. In gas turbine combustors highlyturbulent flows are encountered because of the desired high power density which is achievedby high mass throughputs. Turbulent flows are advantageous because they offer increasedmass and heat transfer which leads to better mixing of fuel and oxidant and finally results inan enhancement of the combustion process.

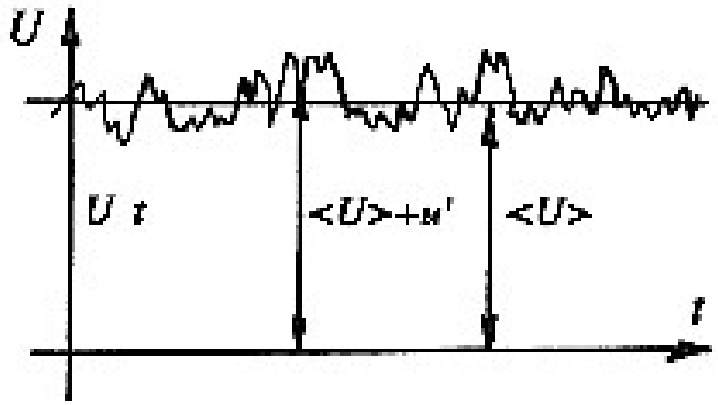

Figure 1.9 Fluctuating Velocities in turbulence

A transition from laminar to turbulent flow occurs when the growth of the flow disturbancesexceeds the damping processes caused by the fluid viscosity. These effects are characterizedby the Reynolds number Red using the following formula

$$Re_d = \frac{U \cdot d}{\nu} \qquad 1.3$$

U is the characteristic velocity [m/s], d is the characteristic dimension [m] and ν is the kinematic viscosity [m2/s].

The transition from laminar to turbulent flow occurs when the
Reynolds number exceeds a certain value. This Red-limit depends strongly on a geometricalconfiguration of the flow. For example the transition from laminar to turbulent flow in asmooth circular pipe occurs when Red > 2300
Where the characteristic dimension “d” is the diameter of the pipe.

The turbulent flow can be characterized qualitatively by (2):

- Irregularity in space and time (chaotic behavior with coherent structures)
- Continuous spectrum of time and length scales
- Large Reynolds numbers
- Three-dimensionality
- Domination of vertical motion
- Intermittency
- Enhanced mass and heat transfer

1.6.1. Statistical description of a turbulent Flow:

The most popular method to describe a turbulent flow field is to use averaged flow parameters (velocity, temperature, pressure). The local turbulent flow is characterized by mean and fluctuating velocity component.

$$\mathbf{u(t) = U + u'(t)} \qquad \mathbf{1.4}$$

Where: $\boldsymbol{U = \frac{1}{N}\sum_i^n u(t)}$ $\mathbf{1.5}$

and $\boldsymbol{\frac{1}{N}\sum_1^n u'(t) = 00\ 01.6}$

The Root Mean Squared Velocity is defined by:

$$\boldsymbol{U_{rms} = \sqrt{\frac{1}{N-1}\sum_i^n (u'(t))^2}} \qquad \mathbf{1.7}$$

The RMS represents the fluctuation of the turbulent velocity (root-mean-square of u'(t)) and it is a measure of the turbulent kinetic energy k. The kinetic energy of a 3- dimensional turbulent flow field (any turbulent flow field) is calculated by using:

$$\boldsymbol{k = \frac{1}{2}\left(u'_{rms}{}^{2} + v'_{rms}{}^{2} + w'_{rms}{}^{2}\right)} \qquad \mathbf{1.8}$$

For 2D geometries:

$$\boldsymbol{k = \frac{3}{2}u'^{2} = \frac{1}{2}\left(u'_{rms}{}^{2} + v'_{rms}{}^{2}\right)} \qquad \mathbf{1.9}$$

The new variable u' is referred to as the turbulence intensity and it represents quasi 3-dimensional velocity fluctuations of the axisymmetric velocity field. It can be used as a rough measure of the turbulent transport. (3)

CHAPTER II:TURBULENT COMBUSTION MODELLING USING OPENFOAM

2.1 Introduction to OPENFOAM :

OPENFOAM is the leading free, open-source software for computational fluid dynamics (CFD). It was created in 1989 and has been managed and developed with new versions being released to the public each year. It's owned by the OPENFOAM Foundation and distributed exclusively under the General Public License.

OPENFOAM is a collection of approximately 150 applications built upon a collection of approximately 150 software libraries (modules). Each application performs a specific task within a CFD workflow. For example, there's an application called `snappyHexMesh` which is a mesh generator for complex geometry, and can generate a mesh around a vehicle.

Figure 2.1 : case directories structure of OPENFOAM

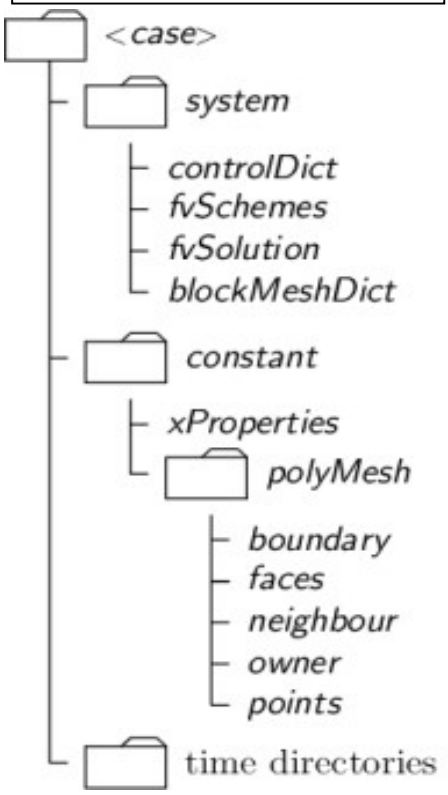

Now, let's talk about the case files. An OPENFOAM case requires definitions for the mesh, initial fields, physical models, control parameters, etc. The case directory consists mainly of 3 directories: `0`, `constant`, and `system`. Here's what each directory contains:

1. **0 directory**: This contains individual files of data for particular fields. The data can be either initial values or boundary conditions that you must specify to define the problem, or results written to file by OPENFOAM.
2. **constant directory**: This contains a full description of the case mesh in a subdirectory polyMesh and files specifying physical properties for the application concerned, e.g., transportProperties.

3. **system directory**: This is for setting parameters associated with the solution procedure itself. It contains at least the following 3 files:
    - controlDict: where run control parameters are set including start/end time, time step, and parameters for data output.
    - fvSchemes: where discretisation schemes used in the solution may be selected at run-time.
    - fvSolution: where the equation solvers, tolerances, and other algorithm controls are set for the run.

2.2 Solver ReactingFoam

ReactingFoam is a solver based on pressure, developed for time-dependent simulations of compressible, reactive flows. It can manage both laminar and turbulent flows with multiple species, taking into account variations in temperature and density (it solves the energy equation). This solver is ideal for simulating combustion processes and chemical reactions in fluids, supporting a range of reaction kinetics and mechanisms for species transport.

The solver employs the PIMPLE algorithm (a combination of PISO and SIMPLE) for coupling pressure and momentum, which draws on the advantages of both PISO and SIMPLE methods for coupling pressure and velocity, ensuring stability when dealing with transient flows with large time steps. It offers the ability to adaptively adjust the size of the time step within different regions through its Local Time Stepping (LTS) feature. It also accommodates Multiple Reference Frames (MRF), models porosity, and facilitates the easy integration of passive scalar transport equations and source terms.

Primarily, this solver is utilized for analyzing burners in the energy sector and for modeling and controlling pollution in environmental engineering. (4)

2.3 Algorithm (PIMPLE):

The PIMPLE algorithm is a method used in Computational Fluid Dynamics (CFD) that combines the strengths of both PISO (Pressure Implicit with Splitting of Operator) and SIMPLE (Semi-Implicit Method for Pressure-Linked Equations) methods. Here's a brief explanation of the algorithm:

1. Set the boundary conditions: This is the initial step where the boundary conditions for the problem are defined.
2. Solve the discretized momentum equation: An intermediate velocity field is computed.
3. Compute the mass fluxes at the cells faces: The mass fluxes are calculated at the faces of the cells.
4. Solve the pressure equation: The pressure equation is solved to get the pressure field.
5. Correct the mass fluxes at the cell faces: The mass fluxes are corrected based on the new pressure field.
6. Correct the velocities: The velocities are corrected on the basis of the new pressure field.
7. Update the boundary conditions: The boundary conditions are updated based on the new velocity and pressure fields.
8. Repeat from step 3: Steps 3 to 7 are repeated for the prescribed number of times.
9. Increase the time step and repeat from step 1: The time step is increased and the entire process is repeated.

The PIMPLE algorithm merges the controls of PISO and SIMPLE, in particular the iterative loops and under-relaxation. All controls are optional; the standard transient algorithm is replicated by deactivating both the under-relaxation and the PIMPLE loop. By including the PIMPLE loop, equations are solved using variables updated within the time step. Accuracy is improved in particular due to the update of matrix coefficients from the contribution of to advection. For transient simulations, temporal accuracy can be maintained at a higher level using a second order time scheme combined with iterations of

the PIMPLE loop. Similarly, the PIMPLE loop can update explicit source terms, e.g. in energy or momentum, to improve accuracy.

PIMPLE can be configured to produce a steady flow solution quickly by a pseudo-transient simulation. These simulations are not intended to capture realistic transient behavior so can run at with some under-relaxation if necessary. The simulations can be accelerated to a steady state using local time stepping (LTS). LTS recognizes that is limited by the maximum associated with the cell with small and/or high. It uses a field of corresponding to the limit in each cell to accelerate the transient solution. While using a field makes the transient solution invalid, it is acceptable at steady state when.

The PIMPLE algorithm is widely used in OPENFOAM. In fact, 59 solvers out of a total of 108 solvers employ this pressure correction algorithm. PIMPLE provides a high level of flexibility using different switches and parameters. All switches and parameters can be set inside the PIMPLE dictionary of fvSolution.

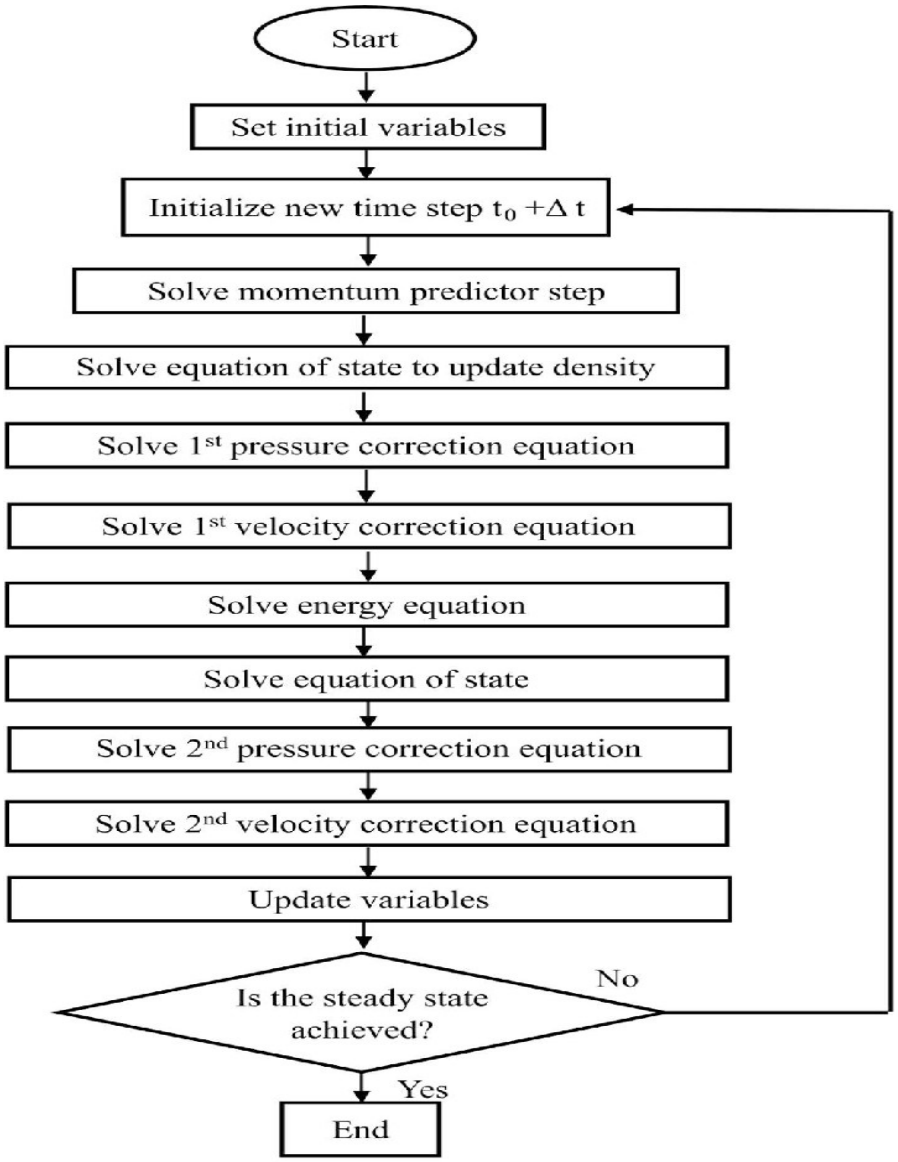

Figure 2. 2 diagram of PIMPLE Algorithm (5)

2.4 Governing Equations:

2.4.1. Continuity Equation:

The **continuity equation** is an expression of conservation of mass. In Cartesian tensor notation, it is written as: (6)

$$\frac{\partial \rho}{\partial t} + \frac{\partial}{\partial x_j}\left(\rho u_j\right) = 0 \qquad 2.1$$

In vector Form it is expressed as:

$$\frac{\partial \rho}{\partial t} + \Delta(\rho \vec{u}) = 0 \qquad 2.2$$

Of course, the grad term will be discredited later.

2.4.2. Navier-Stockes Equation: (Conservation Of momentum):

Physics of fluids and heat transfer as a part of continuum mechanics has now been well established. The nonconservation form of the governing equations in fluids can be derived from the first law of thermodynamics, written as [Truesdell and Toupin, 1960; Chung, 1996]

$$\underbrace{\rho \frac{DV}{Dt}}_{I} = \underbrace{\rho g}_{II} \underbrace{- \nabla p}_{III} + \underbrace{\frac{\partial}{\partial x_i}\left[\mu\left(\frac{\partial v_i}{\partial x_j} + \frac{\partial v_j}{\partial x_i}\right) + \delta_{ij}\,\lambda\,\nabla V\right]}_{IV} \quad \ldots\ldots 2.3$$

Where:

I: Momentum convection

II: Mass force

III: Surface force

IV: Viscous force

Various types of fluid flows emerge from the Navier-Stokes system of equations in nonconservation and conservation forms. In general, computational schemes are dictated from the physics of flows characterized by special forms of the governing equations. (7)

2.4.3. Conservation of Energy:

Conservation of Energy is the first law of thermodynamics which states that the sum of the work and heat added to the **system will result in an increase in the total energy of the system.**

Where **dQ** is the heat added to the system, **dW** is the work done on the system, and **dEt** is the increment in the total energy of the system. One of the common types of energy equation is:

$$\rho\left[\underbrace{\frac{dh}{\partial t}}_{I} + \underbrace{\nabla \cdot (h\,V)}_{II}\right] = \underbrace{-\frac{\partial \rho}{\partial t}}_{III} + \underbrace{\nabla \cdot (k\,\nabla T)}_{IV} + \underbrace{\emptyset}_{V} \qquad 2.4$$

Where h is enthalpy and k is thermal conductivity.

I: Local change with time.

II: Convective term.

III: Pressure work.

IV: Heat flux.

V: Heat dissipation term.

2.4.4. Turbulence Model (Realizable KEpsilon):

There are many two-equation models used in practice today. Among them is the K–ε model, which has been used most frequently for low-speed incompressible flows in isotropic turbulence.

The turbulent viscosity in contains two unknown variables, K and ε. It is therefore necessary that transport equations for K and ε be provided, which can be derived from the momentum equations. To obtain the turbulent kinetic energy transport equation, we take a time average of the product of the fluctuation component of velocity with the turbulent flow momentum equations. After some algebra, we arrive at: (8)

$$\frac{\partial(\rho k)}{\partial t} + \frac{\partial(\rho \overline{u_l} k)}{\partial xj} = \frac{\partial j}{\partial x_j}\left[\left(\mu + \frac{\mu t}{\sigma k}\right)\frac{\partial k}{\partial xj}\right] + Pk + Dk \qquad 2.5$$

$$\frac{\partial(\rho \varepsilon)}{\partial t} + \partial\left(\rho \overline{uj} \varepsilon\right)\partial xj = \frac{\partial}{\partial xj}\left[\frac{\left(\mu + \frac{\mu t}{\sigma \varepsilon}\right)\partial \varepsilon}{\partial xj}\right] + P\varepsilon + D\varepsilon + \rho C1S\varepsilon \qquad 2.6$$

Production Modeling:

Turbulent Kinetic Energy *k*

$$P_k = \mu t\, S^2 \qquad 2.7$$

Turbulent Dissipation Rate *ε*

$$P\varepsilon = C_{\varepsilon 1}\frac{\varepsilon}{k}P_k \qquad 2.8$$

Dissipation Modeling

Turbulent Kinetic Energy

$$Dk = -\rho\varepsilon \qquad 2.9$$

Turbulent Dissipation Rate ε

$$\boldsymbol{D\varepsilon = -\rho C_{\varepsilon 2}\frac{\varepsilon 2}{k+\sqrt{\nu\varepsilon}}} \qquad \textbf{2. 10}$$

Modeling of Turbulent Viscosity **μt**

$$\boldsymbol{\mu t = C\mu\frac{k^2}{\varepsilon}} \qquad \textbf{2. 11}$$

Model Coefficients

$$C\varepsilon 1 = 1.44,\ C\varepsilon 2 = 1.9,\ \sigma k = 1.0,\ \sigma\varepsilon = 1.22.$$

$$\boldsymbol{C1 = max[0.43, \eta\eta + 5]} \qquad \textbf{2. 12}$$

Where: $\boldsymbol{\eta = Sk\varepsilon}$ **2. 13**

$$\boldsymbol{S = \sqrt{2Sij\ SijI}} \qquad \textbf{2. 14}$$

Is the strain rate magnitude.

An improved version of the K–ε model was proposed by Speziale [1987] in which the turbulent stress tensor includes the frame indifferent Oldroyd derivative. (7)

2.4.5. Equation of State:

T he gas constant R used by the perfect gas equation of state is obtained directly from the specie or mixture molecular weight so there is no need to provide an equation of equationOfState enry in the mixture specification.

$$\boldsymbol{\rho = \frac{p}{R\,T}} \qquad \textbf{2. 15}$$

2.4.6. janafThermo:

Calculates Cp as a function of temperature T from a set of coefficients taken from *JANAF* tables of thermodynamics. The ordered list of coefficients is given in Table. The function is valid between a lower and upper limit in temperatureTl and Th respectively. Two sets of coefficients are specified, the first set for temperatures above a common temperature T_c (and below T_h, the second for temperatures below Tc (and above Tl). The function relating c_p to temperature is:

$$\boldsymbol{c_p = R(\left((a_4 T + a_3)T + a_2\right)T + a_1\right)T + a_0} \qquad \textbf{2. 16}$$

In addition, there are constants of integration, a_5 and a_6, both at high and low temperature, used to evaluating h and s respectively. (9)

2.4.7. sutherlandTransport:

Calculates μ as a function of temperature T from a Sutherland coefficient A_s and Sutherland temperature T_s, specified by keywords As and Ts; μ is calculated according to:

$$\boldsymbol{\mu = \frac{A_s \sqrt{T}}{1+(\frac{T_s}{T})}} \qquad \textbf{2. 17}$$

2.4.8. Energy Equation:

The user must specify the form of energy to be used in the solution, either internal energy e and enthalpy h, and in forms that include the heat of formation Δh_f or not. This choice is specified through the `energy` keyword.

$$\boldsymbol{\frac{\partial}{\partial t}(\rho h) + \nabla \cdot (\rho \mathbf{V} h) = -\nabla \cdot \mathbf{q} + \frac{\partial p}{\partial t} + \mathbf{V} \cdot \nabla p + \bar{\bar{\tau}} : \nabla \mathbf{V}} \qquad \textbf{2. 18}$$

where t is time, ρ is mixture density, v is velocity, p is pressure, Yi is the mass fraction of species i, Vi is the diffusion velocity of species i, wi is the mass reaction rate of species i, h is specific total enthalpy of the mixture, and τ is the stress tensor following Stokes hypothesis

We refer to *absolute* energy where heat of formation is included, and *sensible* energy where it is not. For example absolute enthalpy h is related to sensible enthalpy h_s by

$$\boldsymbol{h = h_s + \sum_i c_i \Delta h_f^i} \qquad \textbf{2. 19}$$

where c_i and h_f^i are the molar fraction and heat of formation, respectively, of specie i. In most cases, we use the sensible form of energy, for which it is easier to account for energy change due to reactions. Keyword entries for energy therefore include *e.g.* sensibleEnthalpy, sensibleInternalEnergy and absoluteEnthalpy. (9)

In this work, we used the **sensible Enthalpy** due to the combustion mechanism needed.

2.4.9. sensibleEntalpie :

The sensible enthalpy model is essentially a simplified form of the total enthalpy model. It assumes that only sensible heat is being exchanged and neglects any latent heat effects associated with phase changes.

The equation for sensible enthalpy h can be expressed as:

$$\boldsymbol{h = Cp \cdot T} \qquad \textbf{2. 20}$$

Where:

- h is the sensible enthalpy (J/kg),
- Cpis the specific heat capacity at constant pressure (J/(kg·K)), and
- T is the temperature (K).

This equation represents the energy associated with the temperature of the system, assuming no phase changes occur. It's a simplified form compared to the total enthalpy equation, which would also include terms for latent heat if phase changes were considered.

In OPENFOAM , this model is often implemented as part of the energy equation within the solver, where the energy equation is solved in terms of sensible enthalpy rather than total enthalpy.

2.4.10. Species Transport:

The species transport equation describes the transport of individual chemical species in a fluid flow. It is typically represented by a partial differential equation (PDE) for each species present in the system. The general form of the species transport equation can be written as

$$\frac{\partial(\rho Yi)}{\partial t} + \nabla \cdot (\rho Yiv) + \nabla \cdot (\rho YiVi) = wi \qquad 2.21$$

$$q = -\lambda \nabla T + \rho \sum_{i=1}^{N} hiYiVi \qquad 2.22$$

2.5. How the Composition is calculated? (ODE Ordinary Differential Equations Solvers):

A stiff ODE solver is hence always needed to calculate the composition evolution due to chemical reactions for each computational element, where most combustion and reacting flow studies have centered on backward differentiation formula (BDF) methods]. However, by revisiting the performance of an extrapolation based stiff ODE solver (SEULEX) supported by the KLU sparse matrix math libraries, a recent study has shown that SEULEX always yields higher solution accuracy than CVODE for the same error tolerance, and gives a favorable tradeoff between CPU time and solution accuracy in different reacting flow configurations. (10)

However when simulating this case using the SEULEX solver, it showed an important chance of diverging. Thus a new solver can be used for integration that combines stability and precision: **RosenBrock12**

2.5.1. Rosenbrock12 Method:

Generalisations of the Runge-Kutta method. These consist of implicit methods, where nonlinear equations are solved by Newton iteration at each step, and semi-implicit methods that solve linear equations analogous to .These semi-implicit methods are often called **Rosenbrock** methods. The first good implementation of these ideas was by Kaps and Rentrop, and so these methods are also called Kaps-Rentrop methods.
it seeks a solution of the form:

$$y(x_o + h) = y_o + \sum_{i=1}^{s} b_i k_i \qquad \textbf{2. 23}$$

where the corrections ki are found by solving s linear equations that generalize the structure

$$(1 - \gamma h f') \cdot k_i = hf\left(y_0 + \sum_{j=1}^{i-1} \alpha_{ij} \cdot k_j\right) + hf' \cdot \sum_{j=1}^{i-1} \gamma_{ij} k_j \qquad \textbf{2. 24}$$

i=1,2,...,s

Were we denote the Jacobian matrix by **f** . The coefficientsγ, α_{ij}, ،γ_{ij} , are fixed constants independent of the problem. If D ij D 0, this is simply a Runge-Kutta scheme.

This is only a resume of the Rosenbrock Method, more can be found on (11)

2.6. Numerical Schemes:

Used Limited gauss linear on all the divergence, convective terms, Diffusive terms, Gradient terms to ensure precision and stability.

* Second order accurate.
* Unbounded.
* Excellent choice for isotropic mesh.

The time was set to transient, and the time schemes is Euler: The Euler term represents a first-order accurate approximation of the time derivative. It is straightforward and computationally efficient but may suffer from numerical stability issues, particularly in the presence of stiff or rapidly changing flow phenomena.

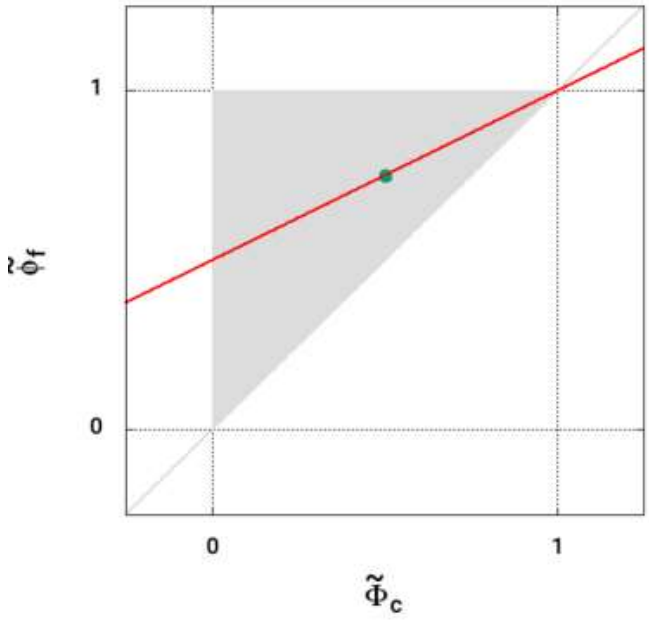

Figure 2. 3 Euler divergence scheme for FVM

$$\boldsymbol{\phi_f = 0.5(\phi_c + \phi_d)} \qquad \textbf{2. 25}$$

.

However, with a good mesh and transient regime we can almost guarantee that the schemes used in this simulation will not cause problems.

2.6.1. Time Scheme:

Concerning the time scheme the Euler Implicit method was used:

Properties

Implicit

First order

Transient

$$\frac{\partial}{\partial t}(\emptyset) = \frac{\emptyset - \emptyset^0}{\Delta t} \qquad \textbf{2. 26}$$

2.7. Chemical Reactions:

2.7.1. Arrhenius reaction Rate:

The **Arrhenius reaction rate** is described by the Arrhenius equation, a mathematical formula that shows how reaction rates in chemical kinetics depend on temperature. The equation is:

$$k = A\,T^{b} \exp\left(-\frac{Ea}{R\,T}\right) \qquad 2.27$$

where:

- **k** is the rate constant, which is the frequency of collisions resulting in a reaction.
- **T** is the absolute temperature.
- **A** is the pre-exponential factor or Arrhenius factor or frequency factor. It represents the number of collisions per second occurring with the proper orientation to react.
- **Ea** is the molar activation energy for the reaction. It is the minimum energy required to initiate a chemical reaction.
- **R** is the universal gas constant.
- **b** is the temperature exponential coefficient..

2.7.2. Third-body Arrhenius reaction rate

The **Third-body Arrhenius gas reaction rate** refers to a three-body reaction in the gas phase of the form:

M is an unspecified collision partner that carries away excess energy to stabilize the AB molecule (forward direction) or supplies energy to break the AB bond (reverse direction). In addition to the generic collision partner M.

Different species may be more or less effective in acting as the collision partner. A species that is much lighter than A and B may not be able to transfer much of its kinetic energy, and so would be inefficient as a collision partner. On the other hand, a species with a transition from its ground state that is nearly resonant with one in the AB∗ activated complex may be much more effective at exchanging energy than would otherwise be expected.

These effects can be accounted for by defining a collision efficiency ϵ for each species, defined such that the forward reaction rate is:

$$k = [A][B][M]k(T) \qquad 2.28$$

Where

$$[M] = \sum_k \varepsilon_k C_k \qquad 2.29$$

Where C_k is the concentration of species k.

2.7.3. Chemistry Reacting Mechanisms Used:

During methane combustion, kinetics plays the same vital role. When comparing different mechanisms, it was found that it is feasible to use reduced schemes in engine simulation, though when elementary chemical reactions are based on Arrhenius law, there are discrepancies of temperature profiles between detailed and reduced mechanisms. Kinetic mechanism for two methane combustion mechanisms is given in Table, while Arrhenius rate parameters are offered in table. (12)

in OPENFOAM , the term Ea/R is directly replaced by Ta where:

The temperature is:

$$Ta = Ea / R \qquad 2.30$$

Table 2. 1 1step and 2 step methane reaction Arrhenius coefficients (12)

Reaction Mechanism	A	m	Ta
Global one-step mechanism			
$CH4+2O2 \rightarrow CO2+2H2O$	$1.5 \cdot 10^{13}$	0	20000
Four-step mechanism			
$CH4+0.5O2 \rightarrow CO+2H2O$	$4.4 \cdot 10^{14}$	0	30000
$CH4+H2O \rightarrow CO+3H2$	$3 \cdot 10^{11}$	0	40000
$H2+0.5O2 \leftrightarrow H2O$	$2.9 \cdot 10^{19}$	-1	40000
$CO+H2O \leftrightarrow CO2+H2$	$2.75 \cdot 10^{12}$	0	20000

1	$H + O_2 = OH + O$	1.59E + 17	−0.927	16874.
2	$O + H_2 = OH + H$	3.87E + 04	2.70	6262.
3	$OH + H_2 = H_2O + H$	2.16E + 08	1.51	3430.
4	$OH + OH = O + H_2O$	2.10E + 08	1.40	−397.
5	$H + H + M = H_2 + M$	6.40E + 17	−1.0	0.
6	$H + OH + M = H_2O + M$	8.40E + 21	−2.00	0.
7	$H + O_2 + M = HO_2 + M$	7.00E + 17	−0.80	0.
8	$HO_2 + H = OH + OH$	1.50E + 14	0.0	1004.
9	$HO_2 + H = H_2 + O_2$	2.50E + 13	0.0	693.
10	$HO_2 + O = O_2 + OH$	2.00E + 13	0.0	0.
11	$HO_2 + OH = H_2O + O_2$	6.02E + 13	0.0	0.
12	$H_2O_2 + M = OH + OH + M$	1.00E + 17	0.0	45411.
13	$CO + OH = CO_2 + H$	1.51E + 07	1.3	−758.
14	$CO + O + M = CO_2 + M$	3.01E + 14	0.0	3011.
15	$HCO + H = H_2 + CO$	7.23E + 13	0.0	0.
16	$HCO + O = OH + CO$	3.00E + 13	0.0	0.
17	$HCO + OH = H_2O + CO$	1.00E + 14	0.0	0.
18	$HCO + O_2 = HO_2 + CO$	4.20E + 12	0.0	0.
19	$HCO + M = H + CO + M$	1.86E + 17	−1.0	16993.
20	$CH_2O + H = HCO + H_2$	1.26E + 08	1.62	2175.
22	$CH_2O + O = HCO + OH$	3.50E + 13	0.0	3513.
23	$CH_2O + OH = HCO + H_2O$	7.23E + 05	2.46	−970.
24	$CH_2O + O_2 = HCO + HO_2$	1.00E + 14	0.0	39914.
25	$CH_2O + CH_3 = HCO + CH_4$	8.91E − 13	7.40	−956.
26	$CH_2O + M = HCO + H + M$	5.00E + 16	0.0	76482.
27	$CH_3 + O = CH_2O + H$	8.43E + 13	0.0	0.
28	$CH_3 + OH = CH_2O + H_2$	8.00E + 12	0.0	0.
29	$CH_3 + O_2 = CH_3O + O$	4.30E + 13	0.0	30808.
30	$CH_3 + O_2 = CH_2O + OH$	5.20E + 13	0.0	34895.
31	$CH_3 + HO_2 = CH_3O + OH$	2.28E + 13	0.0	0.
32	$CH_3 + HCO = CH_4 + CO$	3.20E + 11	0.50	0.
33	$CH_4 + H = CH_3 + H_2$	7.80E + 06	2.11	7744.
34	$CH_4 + O = CH_3 + OH$	1.90E + 09	1.44	8676.
35	$CH_4 + O_2 = CH_3 + HO_2$	5.60E + 12	0.0	55999.
36	$CH_4 + OH = CH_3 + H_2O$	1.50E + 06	2.13	2438.
37	$CH_4 + HO_2 = CH_3 + H_2O_2$	4.60E + 12	0.0	17997.
38	$CH_3O + H = CH_2O + H_2$	2.00E + 13	0.0	0.
39	$CH_3O + OH = CH_2O + H_2O$	5.00E + 12	0.0	0.
40	$CH_3O + O_2 = CH_2O + HO_2$	4.28E − 13	7.60	−3528.
41	$CH_3O + M = CH_2O + H + M$	1.00E + 14	0.0	25096.

[a]Rate constants are in the form $k_n = A_n T^n \exp[-E_n/(RT)]$, here R is the universal gas constant. Units are moles, cubic centimeters, seconds, Kelvins and calories/mole.

Activer Windows
Accédez aux paramètre

Figure 2. 4 41 step reaction of methane Arrhenius coefficients (13)

2.8. Combustion Modeling: Eddy Dissipation Concept (EDC):

.

The eddy-dissipation-concept (EDC) model is an extension of the eddy-dissipation model to include detailed chemical mechanisms in turbulent flows. It assumes that reaction occurs in small turbulent structures, called the fine scales. The length fraction of the fine scales is modeled as: (14)

$$\xi^* = C_\xi \left(\frac{\gamma\epsilon}{k^2}\right)^{0.25} \qquad \textbf{2. 31}$$

where:

* represent fine scale

$C_\xi = 2.1377$ representsvolume fraction constant.

γrepresent kinematic viscosity

The reactions occur in a time scale defined as:

$$\tau^* = C_\tau \left(\frac{\gamma}{\epsilon}\right)^{0.5} \qquad \textbf{2. 32}$$

where $C_\tau = 0.4082$ a time scale constant.

combustion at the fine scales is assumed to occur as a constant pressure reactor, with initial conditions taken as the current species and temperature in the cell. Reactions proceed over the time scale τ^*, governed by the Arrhenius rates of Equation , and are integrated numerically using the**TDAC**algorithm using the **ODE** methods.

in summary:

• A cascade model that describes the energy transfer from larger to smaller scales in turbulent flow

• An energy transfer model that expresses the characteristic quantities for the lowest level of scales as functions of scales from the large-scale level

• The large-scale levels are related to the mean flow by a turbulence model or resolved directly by LES.

• The fine structures are assumed to be a steady-state homogeneous reactor; the chemical reactions occur there

2.9. RadiationModel (P1 Model):

The main assumption of this model is that the directional dependence in the radiative transfer equation is integrated out, resulting in a diffusion equation for incident radiation. Advantages of the P1 model:

• The radiative heat transfer equation is easy to solve with little CPU demand,

• It includes effects of scattering. Effects of particles, droplets, and soot can be included,

• It works reasonably well for applications where the optical thickness is large. (e.g. the model can be used in combustion). (15)

$$q_r = -\delta \nabla G \qquad 2.33$$

Where:

$$\delta = \frac{1}{(3(a+\sigma_s))-C\sigma_s} \qquad 2.34$$

Where **a**is the absorption coefficient, σ_s is the scattering coefficient, **G** is the incident radiation, and **C** is the linear-anisotropic phase function coefficient, described below.

note that **G** needs to be defines , so we introduce it's transport equation:

$$\nabla \cdot (\delta \nabla G) - aG + 4an^2\sigma T^4 + S_g \qquad 2.35$$

The expression for $-\nabla qr$ can be directly substituted into the energy equation to account for heat sources (or sinks) due to radiation.

The P-1 model relies on the following hypotheses:

- The media is optically thick: τ >>1, where τ is the optical thickness defined by the integral of absorption coefficient, κ, along a typical optical path.
- The scattering is linear isotropic.

CHAPTER III: CASE SETUP

3.1 Geometry Description

The liner consists of two coaxial quartz glass tubes (inner quartz glass tube diameter D = 75 mm) which are cooled by forced convection with air. The combustor inlet diameter d is 25 mm. The flame is stabilized aerodynamically via the recirculation of hot flue gases, induced by the combustor geometry with sudden expansion. A hydrogen torch igniter is used to ignite the homogeneously premixed methane/air mixture in the experiment.

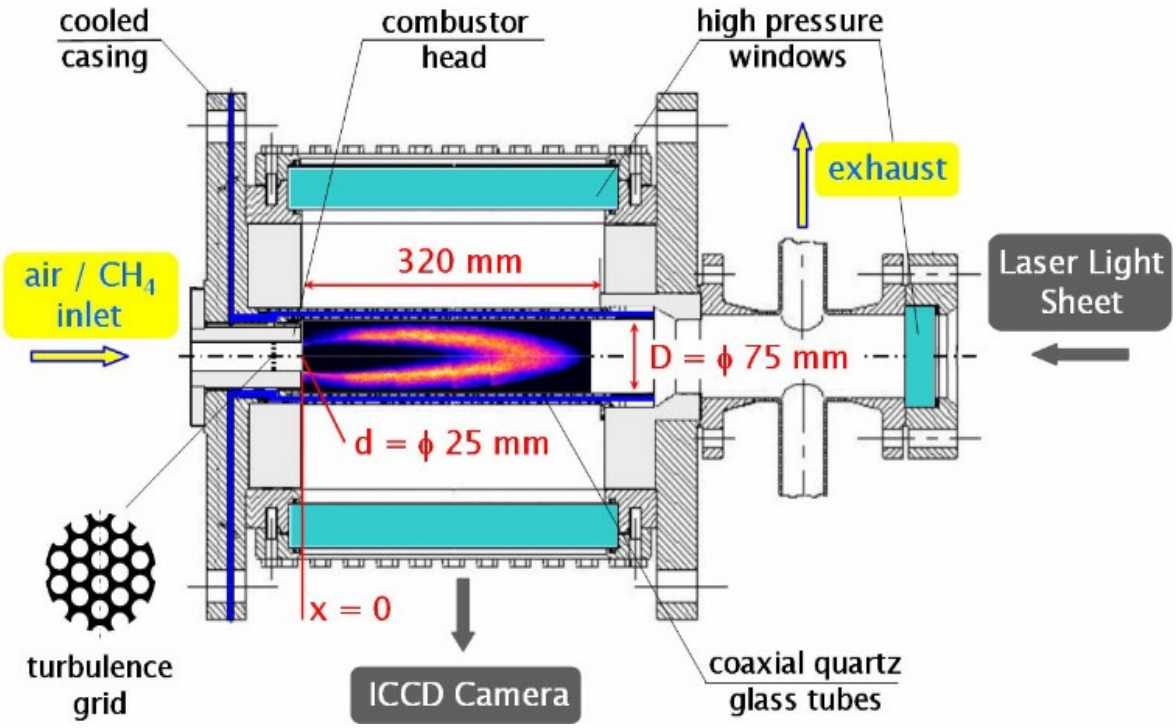

Figure 3. 1 Experimental setup (16)

3.2 Simulated Geometry:

The geometry is a 2D section from the combustion chamber, which can be easily made using **BlockMesh** utility.

Figure 3. 2 geometry of the Combustion chamber

While OPENFOAM only supports 3D Geometries, it can perform a 2D simulation if the conditions are met:

1- The geometry thickness is 1cell.
2- The front and Back planes are defined as empty or wedge.

3.2.1 Boundary Conditions:

The left Segment is defined as Inlet.

The Down segment is defines as symmetry.

The Right Vertical segment is defines as symmetry.

The Front and Back Planes are defined as empty.

All Other segments are defined as wall.

3.3 Mesh

3.3.1 Mesh sensivity :

To ensure the maximum precision with the minimum CPU energy and time cost,, a Mesh Sensitivity Analysis must be done.
taken as a criteria the temperature and the stability, different meshes has been tested.
knowing all the meshes are made with blockMesh Utility,
the **YPLUS** range is respected (between 30 and 100 for realizable K-Epsilon) in all the meshes witch necessities some refinement of the inlet wall side.

Running analyses on each mesh, and record the maxTemperature T for a fixed equivalence ratio $\emptyset = 0.56$ and evaluate the results in terms of time and error range.

Table 3. 1 Mesh sensibility analysis

Elements	Tmax(K)	Error
14980	2133	
15500	2087	0,02156587
17500	2070	0,00814566
35010	2061	0,00434783
70020	2060	0,0004852

3.3.2 Mesh Quality:

Using **BlockMesh utility** a uniform quadratic mesh is created, the cell length is **0.001 (meters)** and this is to ensure stability and reduce the error caused by the tetrahedron mesh.
Note that the thickness is one cell; it is simply because we are in a 2D case.

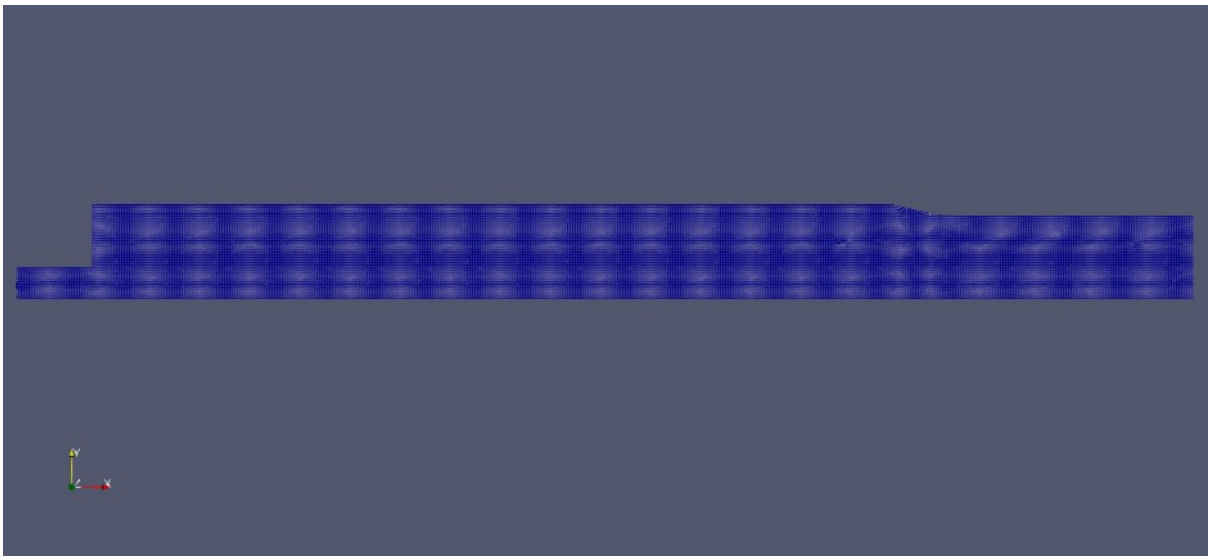

Figure 3. 3 Mesh in paraview (35010 elements)

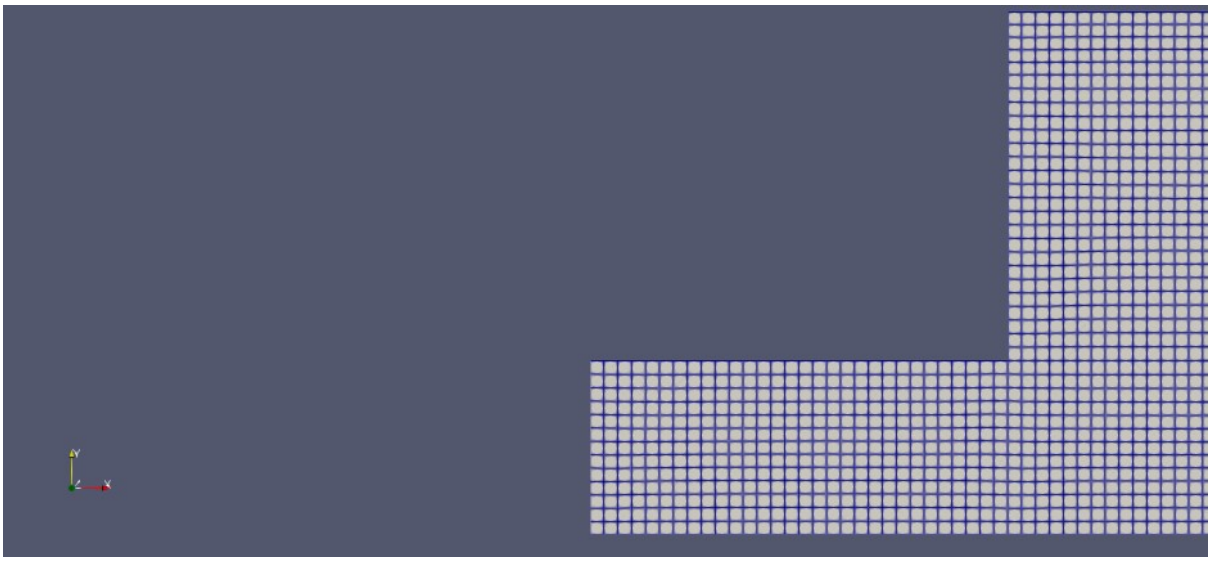

Figure 3. 4 Mesh zoomed on inlet of the combustion chamber

3.3.3 Y Plus analysis

Since we are using Realizable K-Epsilon model, The Y plus margin should be no less than 30 and no more than 300 in the important regions. at our case it has a value of 100 allowing the use of wall functions.

The important region in our case is the small cylinder walls as they the results of the combustion will be incorrect if the k and epsilon values are falsely calculated to the non respect of yPlus Field.

Figure 3. 5 Yplus Field

3.4 Boundary Conditions:

In OPENFOAM , the boundary conditions have to be manually inserted, with a pressure of 5 bar, a temperature of 673 Kelvin and inlet bulk velocity of 40 m/s the values of k and epsilon must be modified exactly to match the experimental setup. The vales taken for k and epsilon are

Most of the boundary conditions used are **ZeroGradiant**, **Uniform**, **WallFunctions** ... depending on the variables expect for some special cases:

the P in outlet:

This got a special care in the outlet region as shown below (taken from P file on openfoam):

```
    outlet
    {
        type            waveTransmissive;
        psi             thermo:psi;
        lInf            1;
        field           p;
        gamma           1.4;
        fieldInf        500000;
        value           $internalField;

}
```

Why the Wave Transmissive Outlet?

Through the testes done to obtain an accepted result, the wave transmissive outlet has proven to be stable in the case of combustion. The other boundaries seem to diverge after the spark.

CHAPTER IV: RESULTS AND DISCUSION

4.1 Non Reacting Flow

4.1.1 Non reacting flow fields

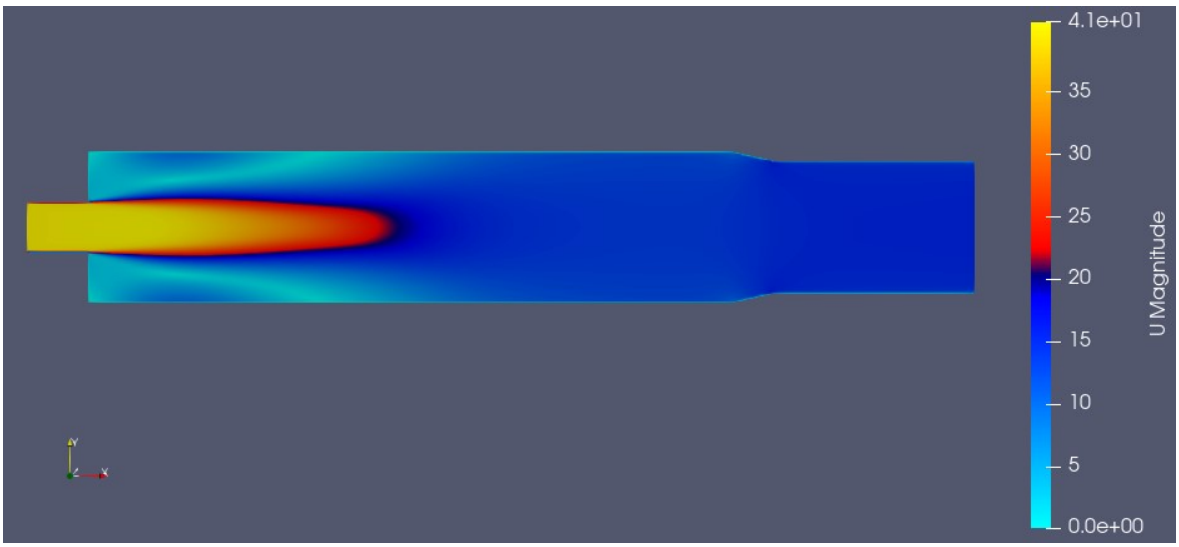

Figure 4. 1 Velocity Field on non reacting Flow

As The Experimental Setup, the Velocity Profile follows the Law of convergent-divergent nozzle, but the strict Student Change in section at the inlet (x=0 mm) generates a turbulence.

The Axial Velocity slows down to envelope the entire volume of the Combustion Chamber.

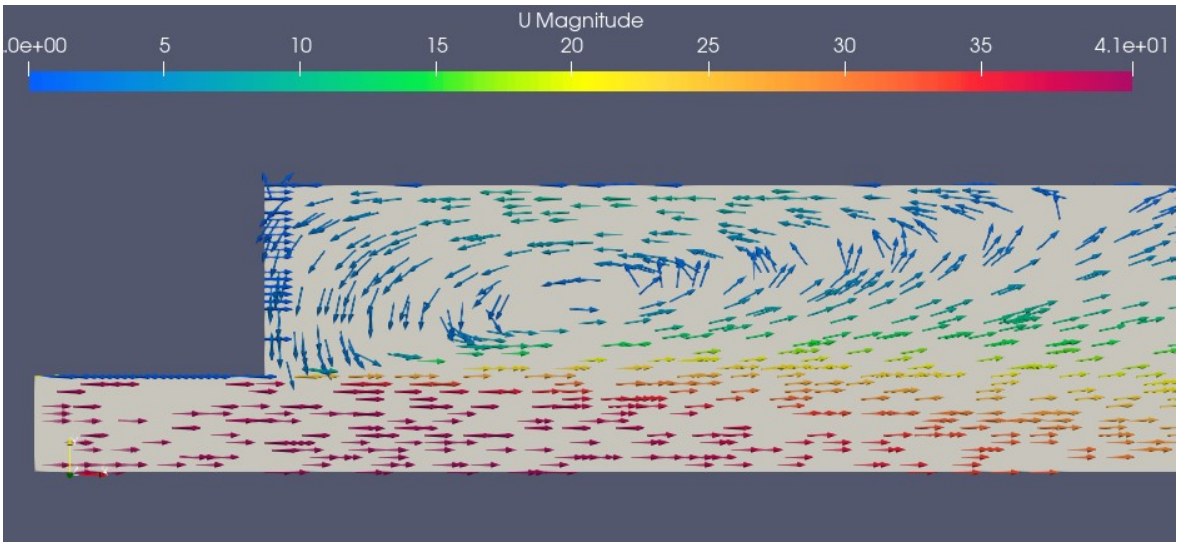

Figure 4. 2 recirculation zone on non reacting flow

The Volume Just after the section Increase has the Vortex phenomenon that last one of the terms of Fluid Dynamics is not wanted as it generated drag and lots of pressure with more dense fluids.

However the vortex phenomenon in the combustion process, is a positive sign especially with a combustion chamber like our case, This Phenomenon is called recirculation zone and it assures the continuity of the combustion Process (chain Reaction).

As theHot Burned Gas gives necessary energy for the unburnt gas to start the ignition. The continuity of combustion is assured by the rotation of the vortex.

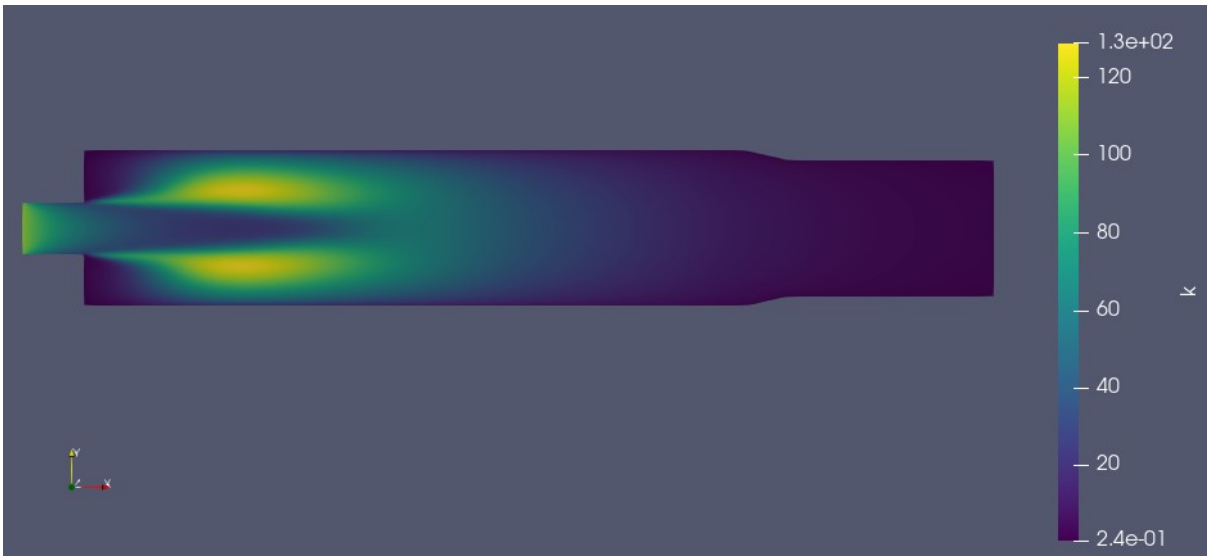

Figure 4. 3 K field on non reacting flow

The figure explains the generation of the K field

+

Figure 4. 4 epsilon field on non reacting flow

4.1.2 Comparison with Published Experimental Data:

all experimental data were obtained thanks to (16)

Two parameters were taken into consideration when comparing with Published experimental data.

- The fist one is the Normalized Axial Velocity:

The axial velocity are directly calculated processed with **Paraview** Post processor and need to be Normalized by the Law:

$$u_{norm} = \frac{U_x}{U_{bulk}} = \frac{u}{40\ m{\cdot}s^{-1}} \quad 3.1$$

- The second one is the NormalizedRoot Mean Squared Velocity which is defined as::

$$RMS_{normalized} = \frac{U\prime}{U_{bulk}} = \frac{U\prime}{40\ m{\cdot}s^{-1}} \quad 3.2$$

Note: The D in the (X/D) refer to the small cylinder (inlet cylinder Diameter) which is 0.025 m

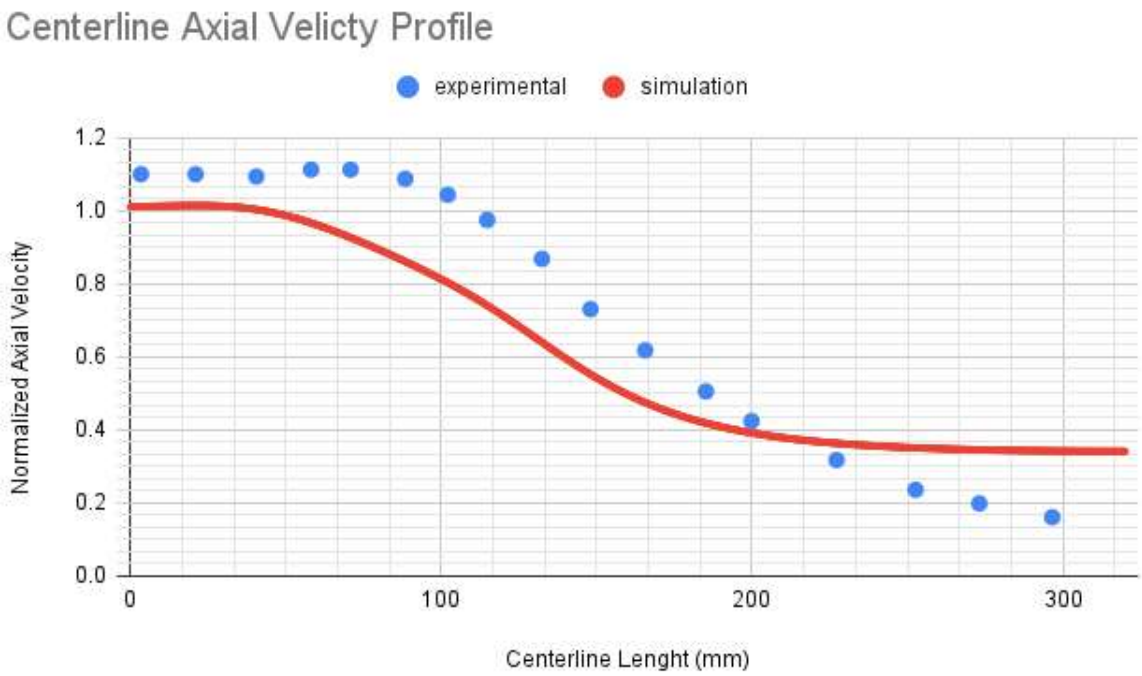

Figure 4. 5 Normalized axial velocity along centerline

The Axial velocity along the centerline is under predicted by the simulation until the zone at x> 200 mm where it shows over-predictions.

The under prediction is due to the a boundary condition of a fixed U value need to be modified to a more complex boundary condition that involves a Velocity Profile that have a maximum value at the centerline r=0.

However the over prediction after x>200 mm is mainly due to the turbulence influence on the Axial Velocity, as the turbulence behavior is not exactly the same (see next figures) the Axial Velocity will surely differ.

In General the results are acceptable

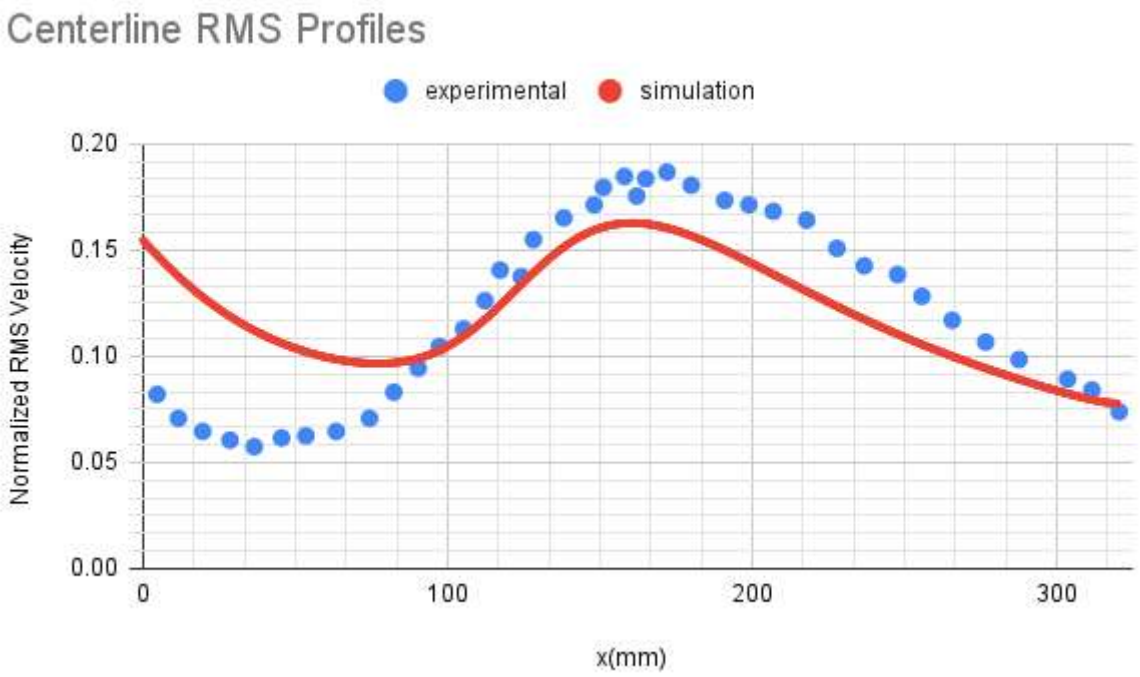

Figure 4. 6 Normalized RMS velocity along centerline

In the second graph, The Figure 4.6 shows the change of the RMS(**Root Mean Squared)** along Velocity along the centerline of the combustion chamber cylinder a major difference is remarkable in the are between x= 0 and x=100 mm. the behavior of the RMS velocity is different as it over predicts turbulence intensity..

However this is expected as the turbulence model used is Realizable K-Epsilon, this last one supposes that the fluctuations of velocities (u', v' and w') behave all the same and that

they are all represented by k (Turbulent Kinetic Energy) and damped by epsilon which is not the real case especially in a confined geometry such this.

For The zone x>100 mm, the simulation mimics the experimental Results with a minor difference.

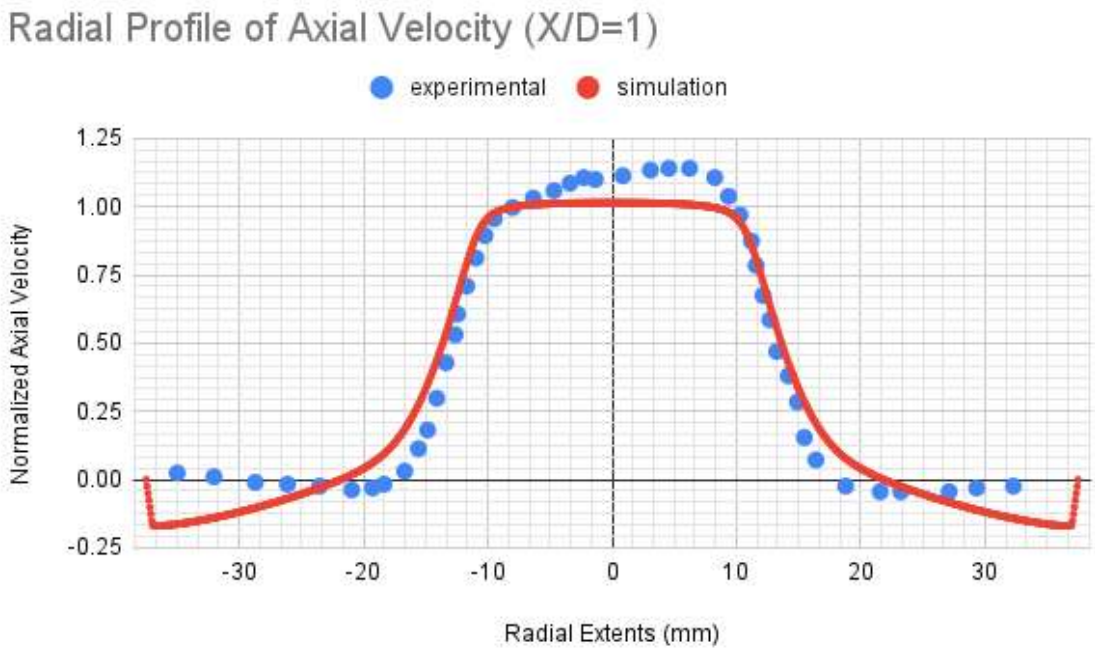

Figure 4. 7 Normalized axial velocity at axial position of (X/D = 1)

The Normalized Axial Velocity in radial extents for the section (X/D) =1: the graph shows a good distribution of the Axial Velocity between the experiment and the simulation.

The negative value of the Normalized Axial Velocity in the radius range within $r = 20\ and\ 30\ mm$ is explained by a The recirculation zone, this backflow region assures the continuity of the combustion process as it transfers the energy from Burnt Gas to the non burnt to start ignition.

the negative axial velocity is more on the simulation compared to published experimental data, but the no Slip boundary conditions corrects that and sets the value of the velocity to 0 at r=0.375

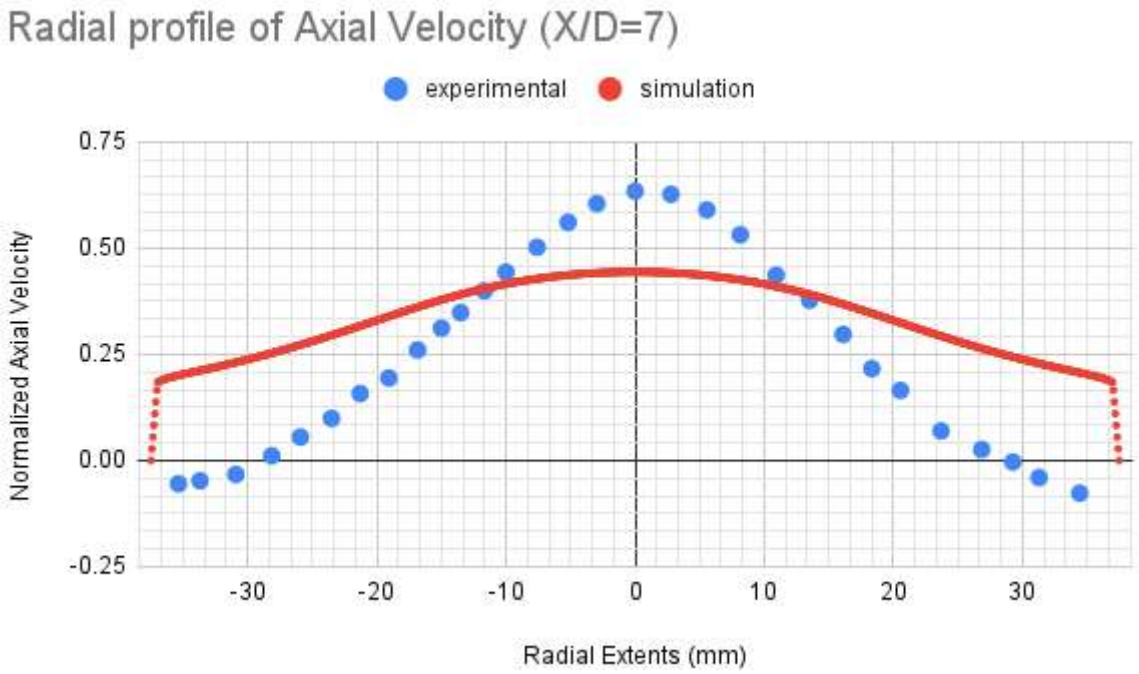

Figure 4. 8 Normalized RMS velocity at axial position of (X/D = 7)

The Figure 4.8 shows the RMS velocity at the axial position X/D = 7 We remark that the depth of penetration of the axial velocity is lower.

The sudden change on the r=0.0375 of axial velocity correspond to the no slip boundary conditions.

The Axial Velocity Profiles are affected by the Fluctuating velocities represented by k.

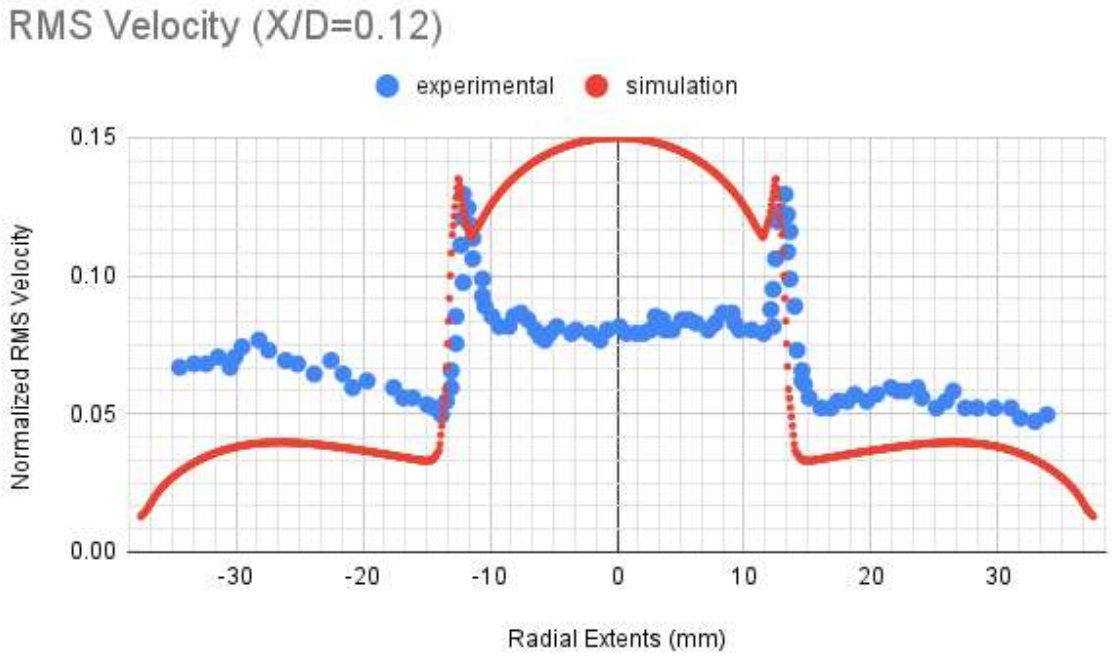

Figure 4. 9 Normalized RMS velocity at axial position of (X/D = 0.12)

In the Figure 4.9: the simulation over-predicts the Turbulence intensity (represented by the RMS velocity) at the jet core r=0 to r= 15 mm.

While an under prediction is remarked on the extremities of the combustion chamber

These unmatched results are explained by the uncertainty of the boundary conditions with the inlet flow.

The RANS Model at the combustion chamber inlet does not mimic the experimental, which is expected as it is one of the weaknesses of RANS. (17).

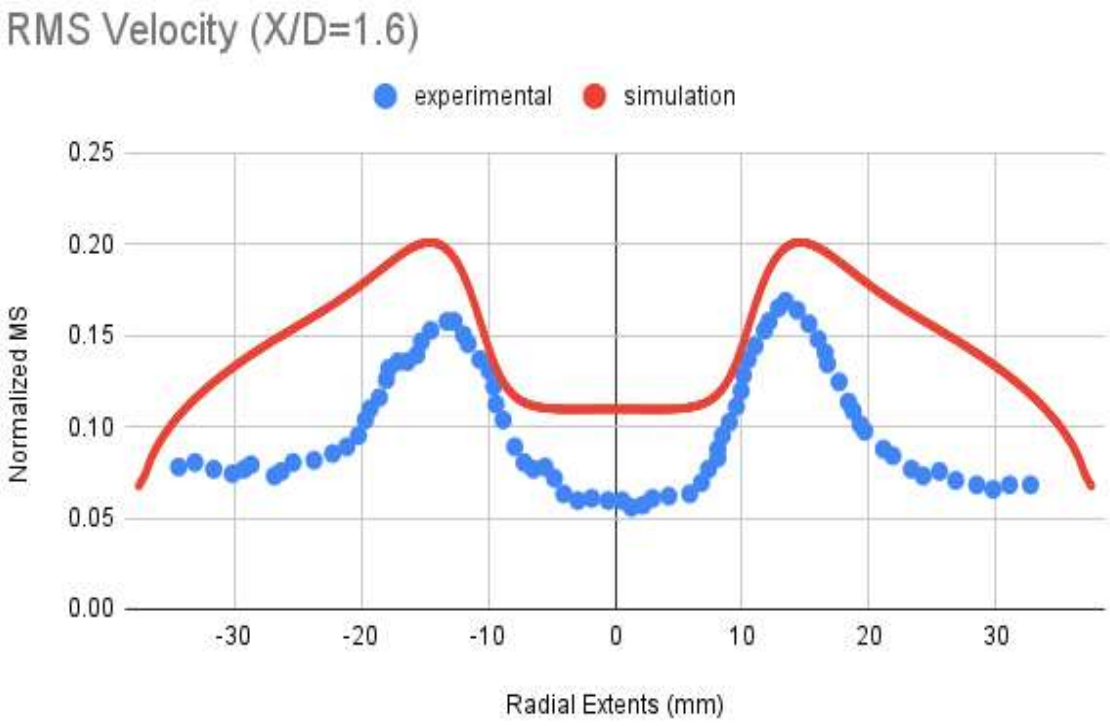

Figure 4. 10 Normalized RMS velocity at axial position of (X/D = 1.6)

In the Figure 4.10 the simulation curve here takes the form of the experiment's curve, but in terms of accuracy it lacks the precision.

The simulation over predicted the values of the RMS velocity, but in general this results are acceptable as it is a RANS simulation, the eddies are not modeled but just are represented by a scalar K and by a dissipation rate epsilon.

We can conclude that the realizable k-epsilon model starts to mimic the behavior of a real turbulence at that section of the combustion chamber.

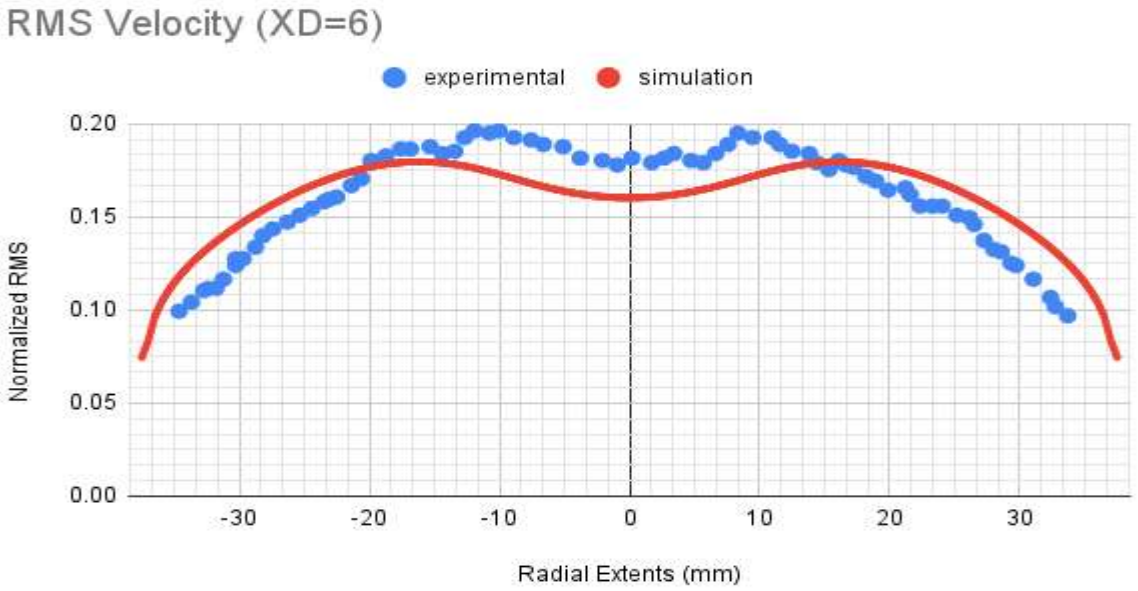

Figure 4. 11 Normalized RMS velocity at axial position of (X/D = 6)

The Figure 4.11 shows the RMS velocity at section x/d = 6

The Model simulates the turbulence well keeping the shape of the experimental graph.

The results are good in this section. We remark a little over estimation of the jet breakup at the jet core. (Under estimation of RMS) but it is neglected.

The model matches reality well at this stage.

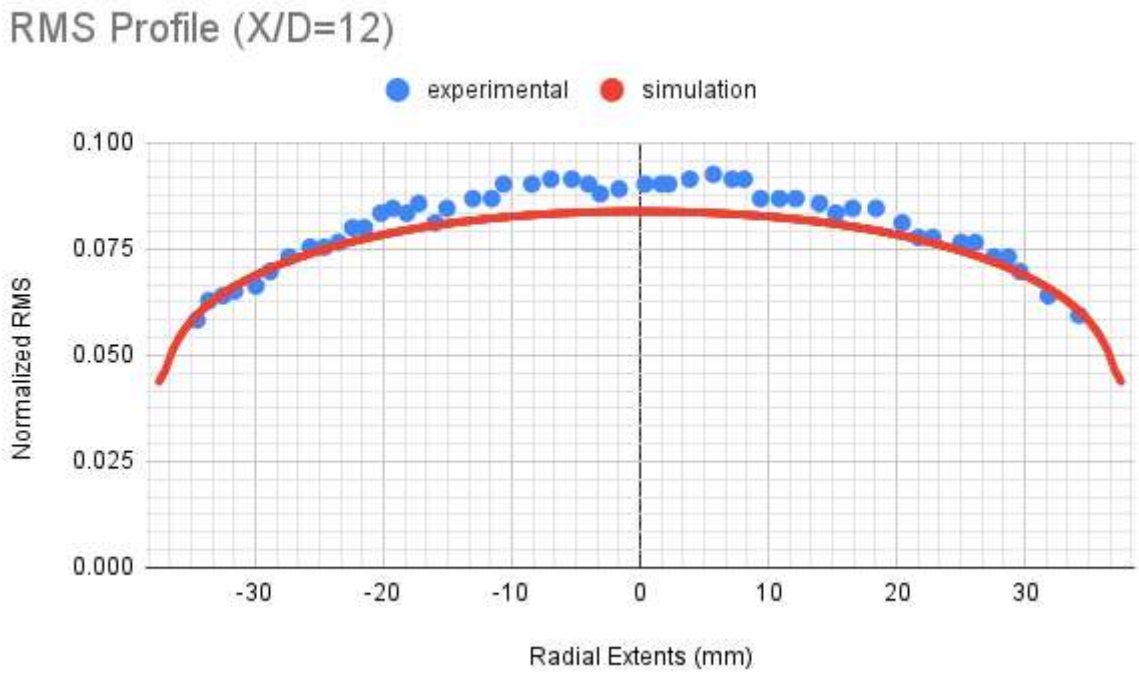

Figure 4. 12 Normalized RMS velocity at axial position of (X/D = 12)

The figures represents the normalized Root Mean Squared Velocity in function of radial extents at the position X/D = 12, the graph of simulation matches the experimental results perfectly.

Conclusion:

The model (realizable k epsilon) well predicted the behavior of the turbulence energy, but in the regions with sudden change of section area, the model tend to have some error
The error of the turbulent velocity fluctuations does affect the velocity itself resulting on a change of velocity profile

This is explained briefly by the phrase:
One limitation of the realizable k-epsilon model is that it produces non-physical turbulent viscosities in situations when the computational domain contains both rotating and stationary fluid zones (e.g., multiple reference frames, rotating sliding meshes). This is due to the fact that the realizable k-epsilon model includes the effects of mean rotation in the definition of the turbulent viscosity (18).

The error produced by the RANS (realizable k epsilon) model, may be attributed to the entrainment of the shear-layer turbulence with the dissipating grid turbulence in the jet core. This leads to a complex, anisotropic interaction before the effects of the grid turbulence completely dissipate. The nature of these interactions (perhaps amplified by the confinements) is probably difficult to model, under the assumption of isotropy in RANS, and appears to demonstrate that even a 'simple' geometry such as this requires a scale-resolving approach such as LES to account for the flow physics.

4.2 Reacting Flow:

4.2.1 Reacting Flow Fields:

Recap:

The kappa κ Field is the Main Important role in the EDC combustion model
Eddy Dissipation Concept (EDC):

The EDC model focuses on combustion reactions occurring in regions of the flow where turbulence dissipates kinetic energy. These regions are often referred to as “fine structures.”

The Significance of kappa:
kappa is a dimensionless factor that influences the reaction rate in EDC.

Essentially, kappa modulates the reaction rate based on local turbulence conditions. High turbulence leads to uniform reactions, while low turbulence accounts for fine-scale variations.

- Higher kappa values imply more uniform reaction rates, assuming well-mixed combustion.
- Lower kappa values allow localized variations, capturing fine-scale turbulence effects.

By adjusting kappa, EDC provides a more accurate representation of real-world combustion processes.

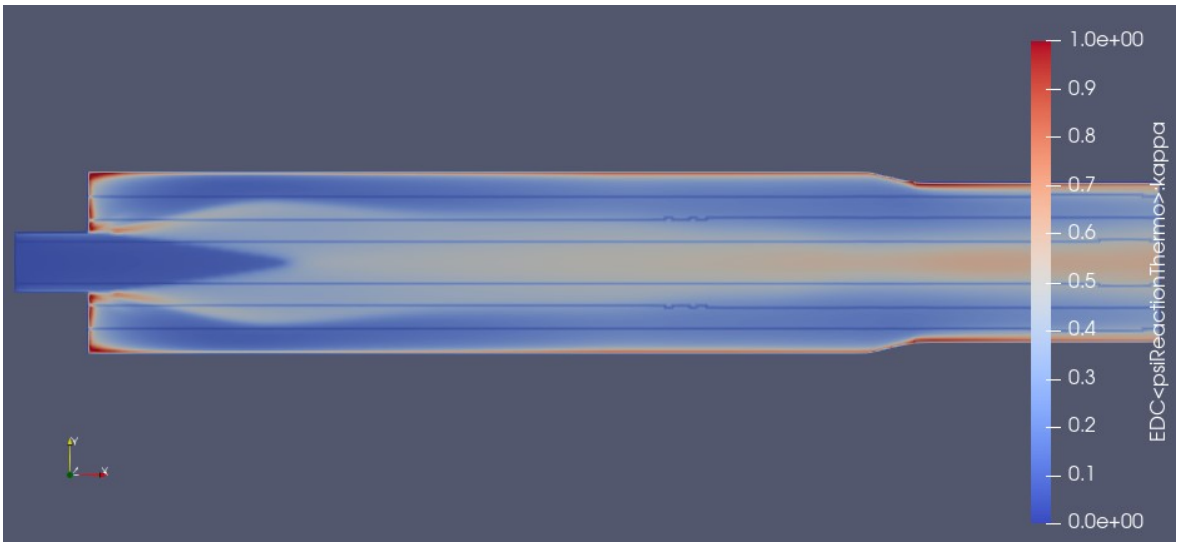

Figure 4. 13 kappa field on reacting flow at Φ=0.56

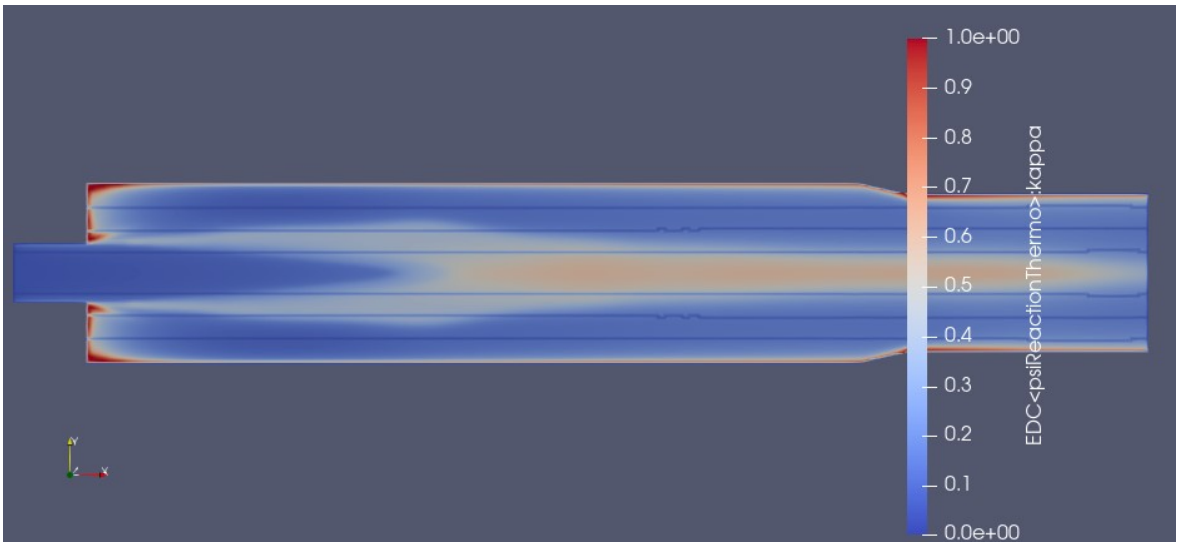

Figure 4. 14 kappa field on reacting flow at Φ=0.43

In The Simulation results the kappa field already takes the shape of the flame even on the Non Reacting Flow.

This conclude that the reactions and heat release will be maximal at $\kappa = 1$ and non excising at $\kappa = 0$.

It is remarkable that:

- The Wall Regions have a high kappa value.

The kappa > 1 regions are shaped like the premixed flame shape

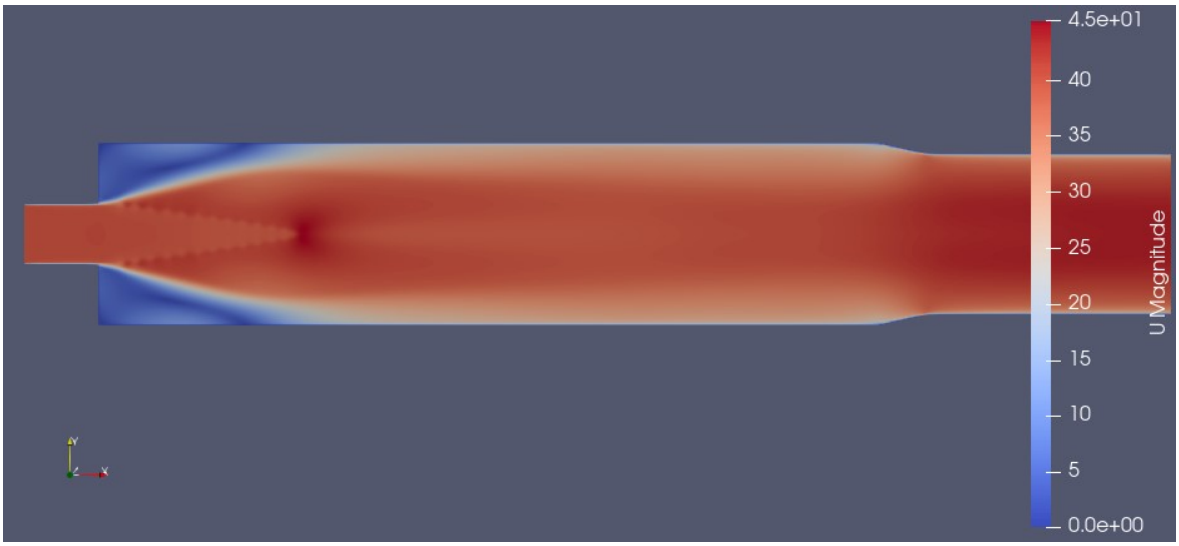

Figure 4. 15 Velocity (m/s) field on reacting flow at Φ=0.56

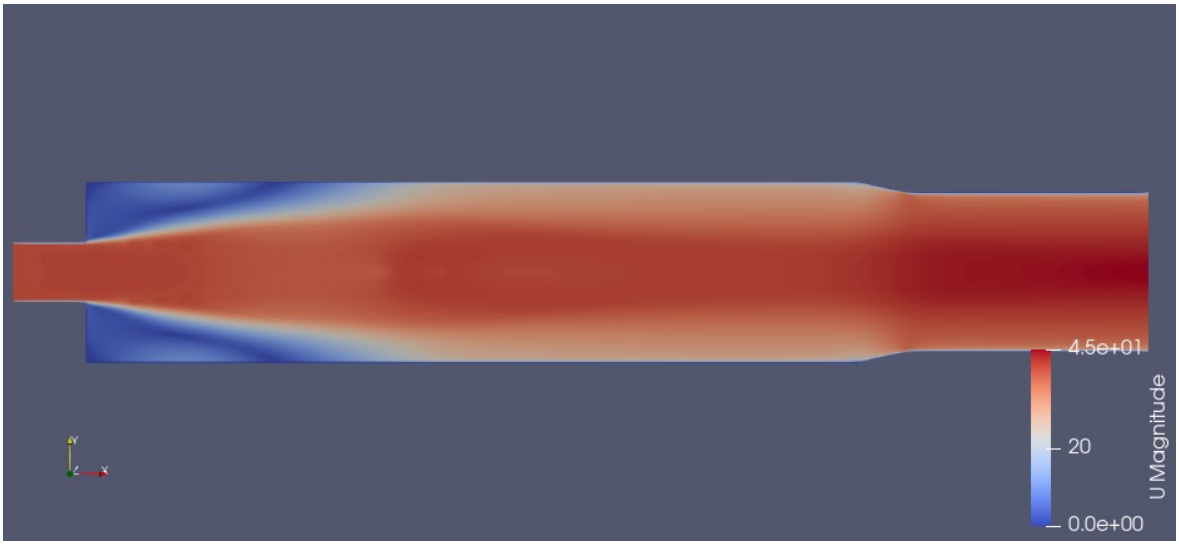

Figure 4. 16 Velocity (m/s) field on reacting flow at Φ=0.43

The figures 4.16 and 4.17 shows the change of velocity field in the equivalence ratios 0.56 and 0.43, it it remarkable by comparing to the non reacting Flow, that an acceleration of velocity has occurred in the combustion chamber.

The increased velocity takes the shape of a cone in the left volume of the combustion chamber, that code is dependent on the equivalence ratio.

The shape of the Cone is more divergent for an equivalence ratio of 0.56, and this is easily predictable due to the fact that the combustion in that condition releases more energy than

the one with equivalence ratio of 0.43, thus this energy which was originally heat (intern energy) will be converted much faster to a kinetic energy of the fluid.

This is important in the field of designing the combustion chambers, as these velocities affect the drag coefficient thus the erosion of the combustion chamber inner wall. This is a subject of research itself

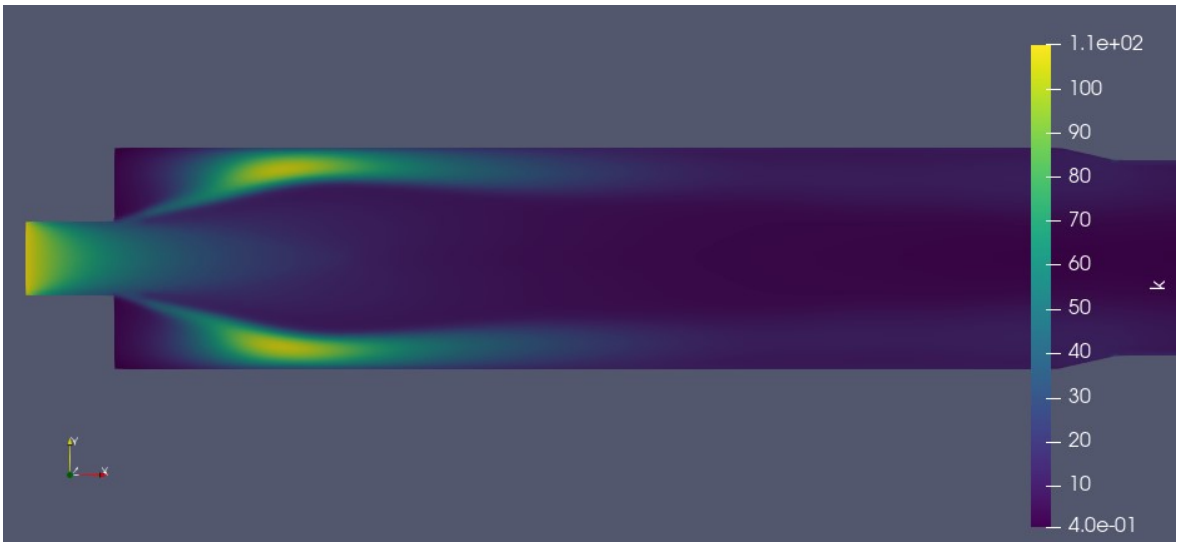

Figure 4. 17 k field on reacting flow at Φ=0.56

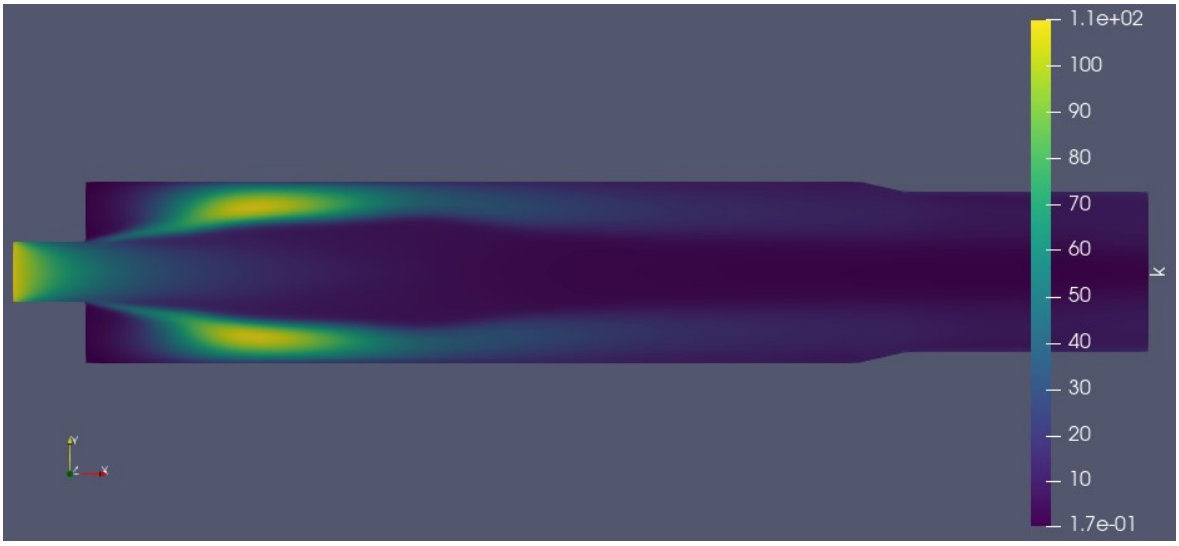

Figure 4. 18 k field on reacting flow at Φ =0.43

These Figures 4.17 and 4.18 shows the turbulence kinetic energy (k) field of both 0.56 and 0.43 equivalence ratios, a difference in the distribution of k is remarkable compared to the non reacting flow.

As k is more narrow in the Φ =0.43 reaction. Despite the fact that both of the equivalence ratio combustions have the same boundary conditions.

This illustrate that the combustion process change the behavior of the fluid

Figure 4. 19 Epsilon field on reacting flow at Φ = 0.56

Figure 4. 20 Epsilon field on reacting flow at Φ = 0.43

The Epsilon field however doesn't show a big difference in terms of value nor distribution as it is largely linked to wall conditions where the majority of dissipation occurs.

Figure 4. 21 O2 mass fraction field in reacting flow Φ = 0.56

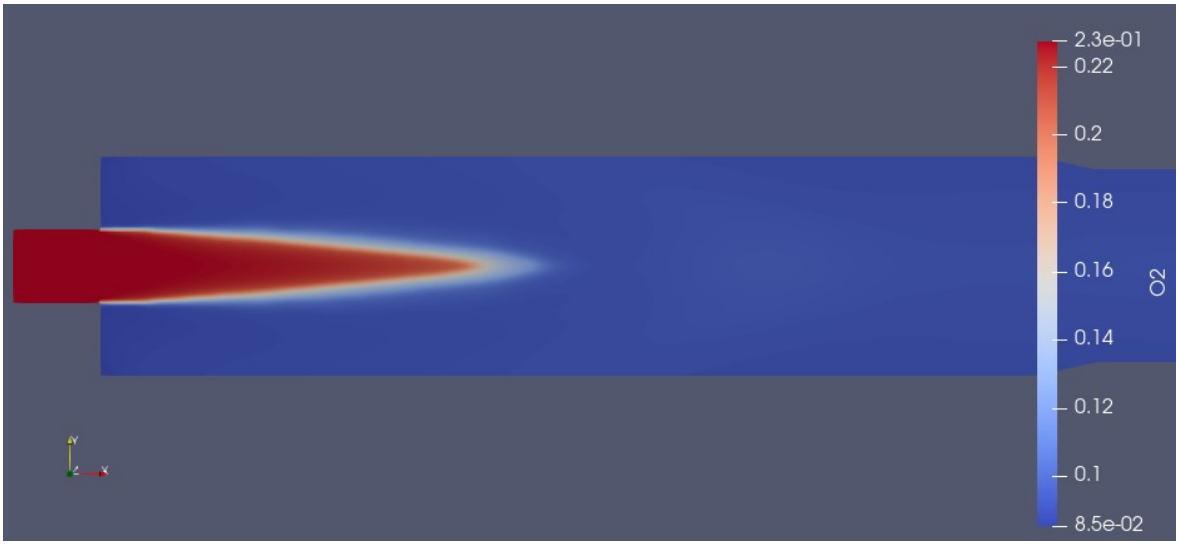

Figure 4. 22 O2 mass fraction field in reacting flow Φ =0.43

The figures 4.22 and 4.21 illustrate the contour of the mass fraction of the O2 molecule, It may be confusing that the inlet value is the same for all reaction, but OPENFOAM round up the values as the inlet O2 mass fraction value is 0.2257 and for Φ =0.43 is 0.227 which ParaView rounds up to 0.23 in the post processing.

However the OPENFOAM takes this in consideration and calculates with the exact values in double precision by default.

This is proven by the differences of flame shape and the temperature difference; also by the mass fraction after the combustion as (at the outlet) as the oxygen that did not react absorbs the heat from the reaction. 0.085 for Φ =0.43 and 0.11 for Φ =0.56

Figure 4. 23 CH4 mass fraction field in reacting flow Φ = 0.56

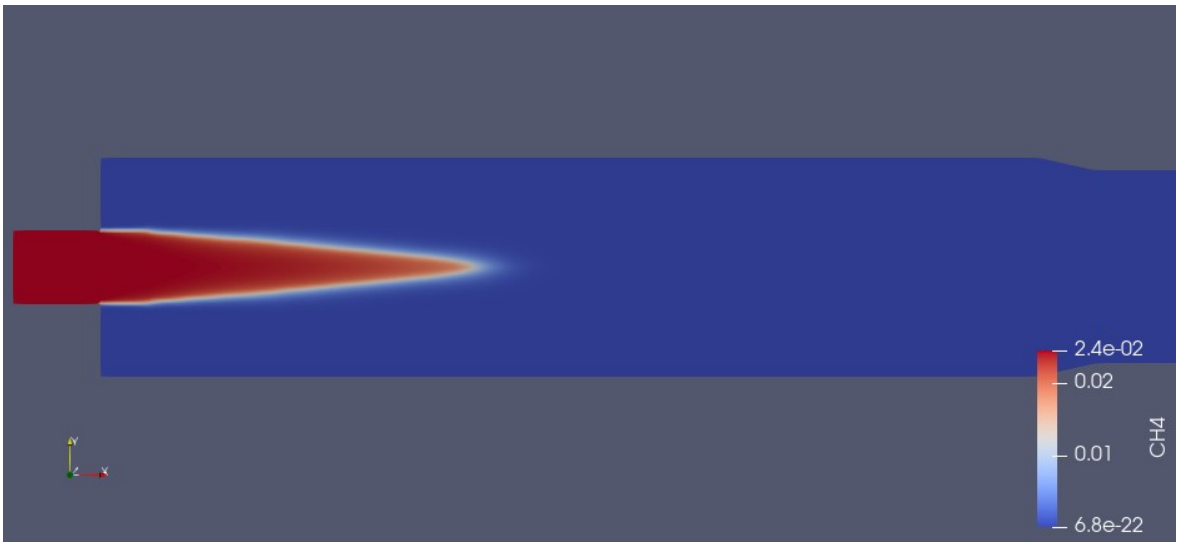

Figure 4. 24 CH4 mass fraction field in reacting flow Φ = 0.43

The same is being said for the figures 4.23 and 4.24 except the fact that all the CH4 reacts

4.2.2 Comparison with Published experimental data (19)::

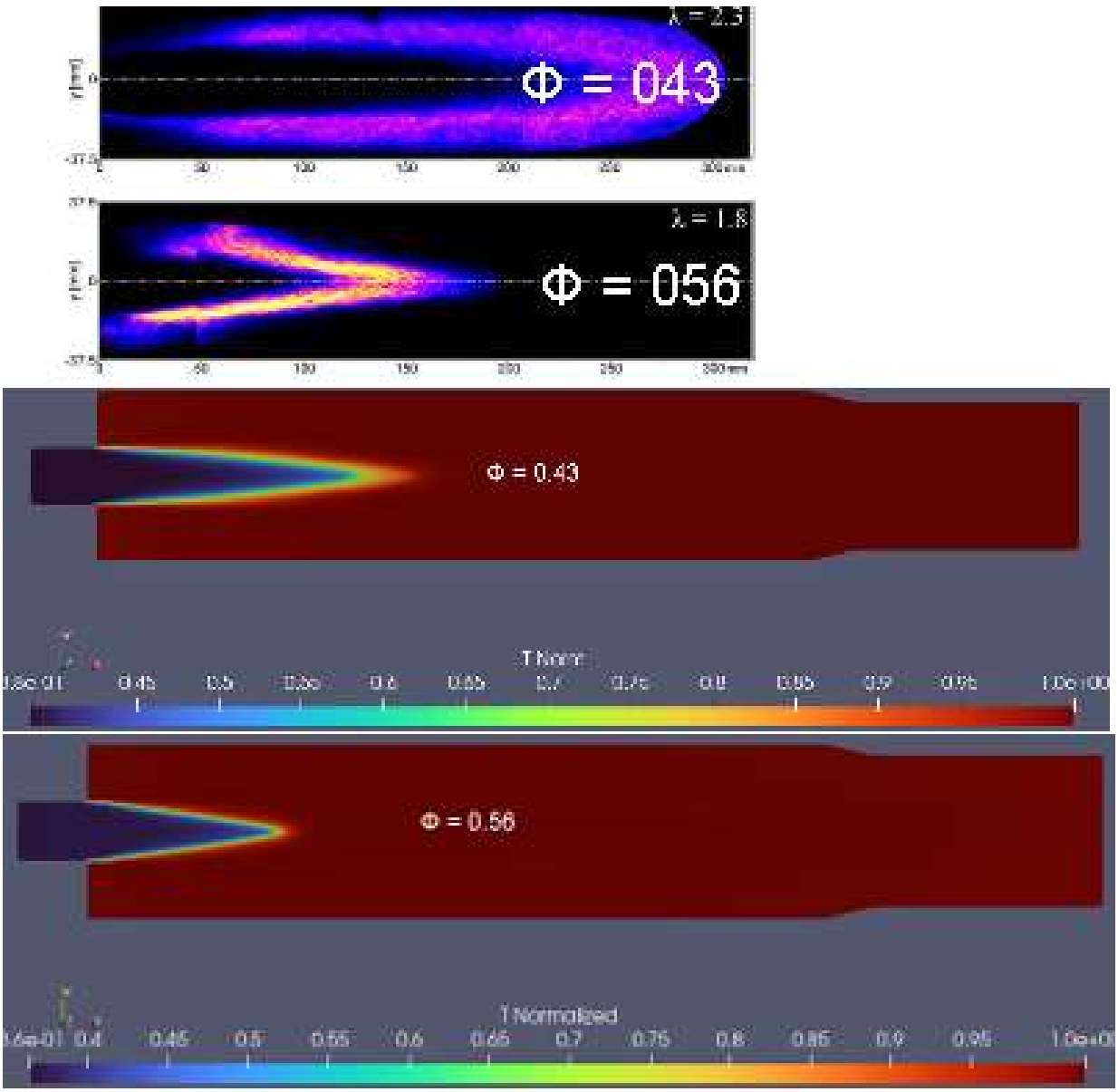

Figure 4. 25Comparison of the temperature Field in the simulation and the flame length in published experimental data for the equivalence rations O2 field in reacting flow Φ = 0.56 and 0.43

The Figure 4.25 illustrates the Comparison between flame length between the published experimental data and the simulation for the equivalence rations of 0.56 and 0.43.
The two upper images represent the published experimental data; the two lower ones are the simulations.

The k-ε model represented shows reduction in flame length which is the case in the published experimental data; however both flame lengths were shorter than the experiment.

This is largely a consequence of the fact that the RANS-EDC combination does not account for fluctuations of the temperature and species concentrations on the reaction rate. The striking feature of this comparison is that the RANS predicts the flame to have a considerably reduced flame brush, compared to the experiments how the flame to fluctuate over a significant length of the combustion chamber length at the lean equivalence ratio.

4.3 Influence of equivalence ratio on the combustion temperature:

To study the effect of the equivalence ratios on the temperature of combustion, an automation is recommended, thus this python program was created to It is due to the fact that reactingFoam solver works with mass fractions in chemistry and even the post processing.

```
def calculate_mass_fractions(phi_values):
    with open("mass_fractions.txt", "w") as file:
        file.write("phi\tCH4\tO2\tN2\n")
        for phi in phi_values:
            mt = 16 + (2 / phi) * (32 + 28 * 3.76)
            mch4 = 16 * 1
            mo2 = 2 * 32 / phi
            mn2 = 3.76 * 2 * 28 / phi
            ych4 = mch4 / mt
            yo2 = mo2 / mt
            yn2 = mn2 / mt
            file.write(f"{phi:.2f}\t{ych4:.6f}\t{yo2:.6f}\t{yn2:.6f}\n")

phi_values = [0.25, 0.35, 0.45, 0.55, 0.65, 0.75, 0.85, 1, 1.1, 1.2, 1.3, 1.4, 1.5, 1.6, 1.7]
calculate_mass_fractions(phi_values)
print("Results written to mass_fractions.txt")
```

Figure 4. 26 python program of mass fractions of reactors

The output of the program shown in Fig 4.26 is a file named mass_fractions.txt shown below:

The flame temperature was calculated using OPENFOAM simulation then manually was manually put into its corresponding equivalence ratio, see Table 4.1.

Table 4. 1 mass fractions of reactants for different equivalence ratios

equivalence ratio	Y(CH4)	Y(O2)	Y(N2)
0.25	0.01436	0.229753	0.755887
0.35	0.019989	0.228441	0.751571
0.45	0.025554	0.227144	0.747303
0.55	0.031056	0.225861	0.743083
0.65	0.036496	0.224593	0.738911
0.75	0.041876	0.223339	0.734785
0.85	0.047196	0.222099	0.730705
1	0.055066	0.220264	0.72467
1.1	0.060241	0.219058	0.720701
1.2	0.065359	0.217865	0.716776
1.3	0.070423	0.216685	0.712893
1.4	0.075431	0.215517	0.709052
1.5	0.080386	0.214362	0.705252
1.6	0.085288	0.21322	0.701493
1.7	0.090138	0.212089	0.697773

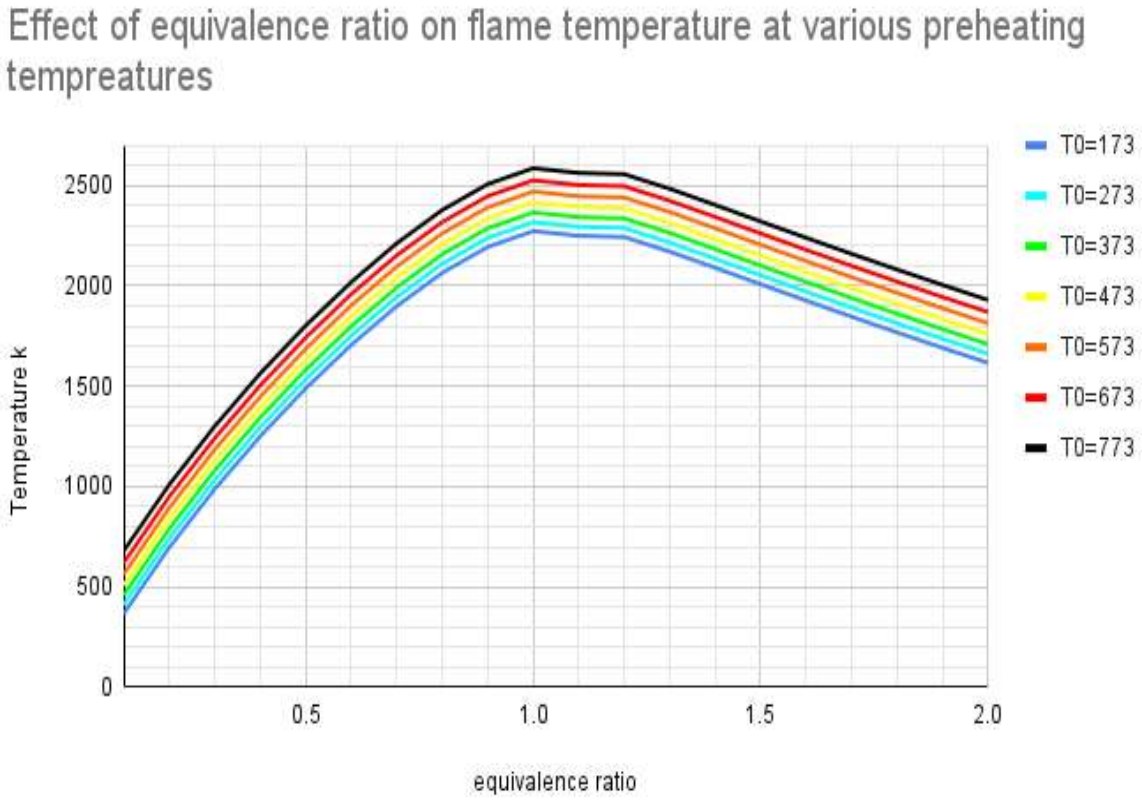

Figure 4. 27 Effect of equivalence ratio on flame temperature at various preheating tempreatures

From 4.27, it is shown that the combustion temperature first increases and then decreases with the increase of the air-fuel ratio, and the maximum value appears around 1.

At low-fuel ratio, natural gas is not burned completely because of the lack of air, a large number of incomplete combustion products are produced, and the combustion temperature is much lower than the stoichiometric.

Gas combustion can be ensured by increasing air volume, but too much gas volume increase. The flue gas takes away a lot of heat, resulting in the temperature drop.

Effects of preheating temperature:

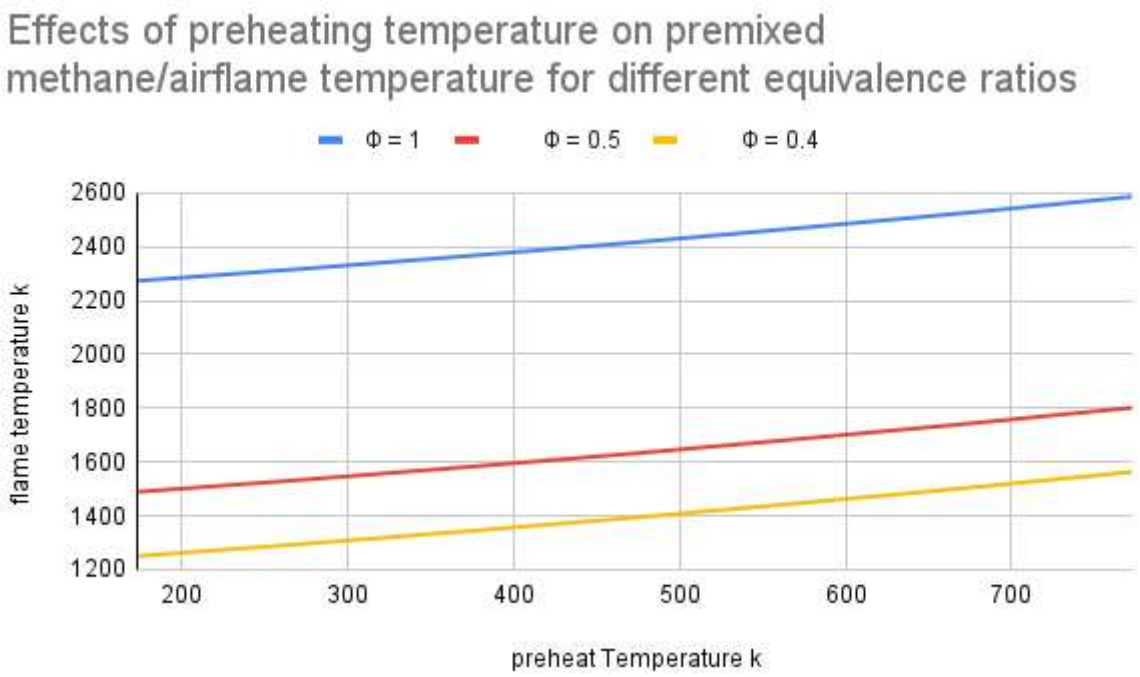

Figure 4. 28 Effect of air preheating temperature on flame temperature

.

From the graph on Figure 4.28, it is evident that the temperature of combustion chamber increases gradually with the increase of preheated air temperature. The temperature of the combustion chamber can reach 2100 K at maximum.

The combustion temperature rises slowly when the preheated air is below 500 K and the temperature rise rate is about 17-28 degrees for every 100 degrees increase. The combustion temperature increases rapidly with the increase of preheated air temperature, after preheating temperature of 600 K and the rise rate increases to 40-47 degrees for every 100 degrees increase.

If the air preheating temperature is higher, the combustion temperature is higher. However, temperature will lead to a rapid increase in NOx content in the flue gas. (20)

Validation with experimental results:

the experimental results obtained from (21) shows a very close results thus validating the mechanisms the the reaction foam combustion model and OPENFOAM

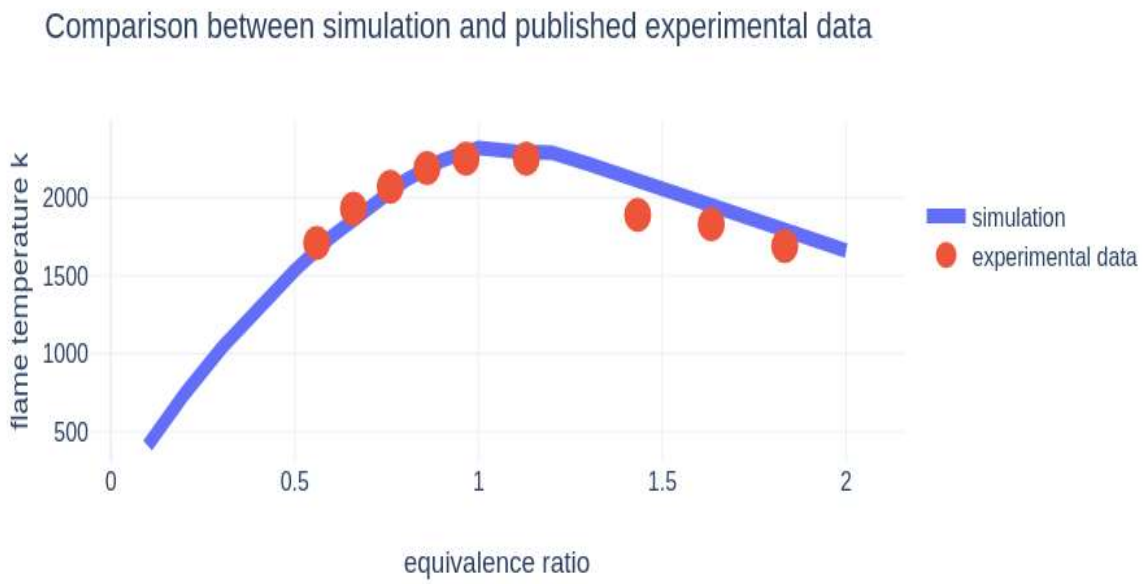

Figure 4. 29Comparison between simulation and published experimental data (21)

Although the article mentioned earlier studied(21) in general the reduction mechanisms, it is wise to compare our results.
The graphs at Figure 4.29 show a very close results knowing that our simulation did not use a reduction mechanism nor a tabulation method, thus this precision is expected.
with a little over prediction of temperature that may be generated by the heat loss in the experimental process.

Conclusion:

The flame length at φ = 0.56 was shorter compared to the experiment see Fig4.25. We infer that the reaction-rates were over-predicted as these flames are closer to the flamelet region which the k epsilon has an error to model the turbulence parameters there.

The model predicted the strongly finite-rate driven lean flame, at φ = 0.43, with a shorter flame length. Here, we believe the EDC assumptions were more justified since the flame is entirely in the highly turbulent shear layer and stabilization is more due to the entrainment by vortices generated by the shear layer than by those generated by the turbulence grid.

This over-prediction is attributed to the EDC strategy for the reaction rate closure at low Re.

According to the results of figures 4.27 and 4.28,

The combustion temperature can reach the highest value by controlling the equivalence ratio around 1 which accords with the theory and with the published experimental results (20).

The increase or decrease of equivalence ratio can reduce the temperature, increasing the amount of air decreased of the heat release, and decreasing the amount of air resulted in incomplete combustion. The combustion temperature can be increased by increasing the temperature of preheated air. The temperature rise rate is about 35 K for every 100 degrees increase below 500 K, and by average 55 K for every 100 K increase after 500 K.

General Conclusion

In this study, we used the open-source computational fluid dynamics software OPENFOAM to simulate turbulent premixed combustion of a methane/air mixture. The mathematical model we employed is based on solving the Navier-Stokes equations with turbulence modeled using the RANS approach (specifically, the k-epsilon realizable approach). We examined a detailed chemical mechanism consisting of 41 reactions for two equivalence ratios ($\varphi = 0.56$ and $\varphi = 0.43$), which were derived from published experimental data. The mixture was preheated to 673 K, at a pressure of 5 bars, and a jet velocity of 40 m/s.

The results indicate that the model provided a better match with the experimentally measured flame length for an equivalence ratio of $\varphi = 0.43$. This suggests that the model is adequate when finite rate effects are dominant, but adjustments may be necessary for flames closer to the flame regime. The realizable k-epsilon model effectively predicts turbulence energy behavior, but it exhibits errors in regions with sudden changes in section area. These errors lead to inaccuracies in turbulent velocity fluctuations and resulting velocity profiles.

Regarding combustion modeling, the flame length at an equivalence ratio of $\varphi = 0.56$ was found to be shorter than the experimental results. This discrepancy indicates over-predicted reaction rates due to errors in modeling turbulence parameters in the flamelet region. Conversely, the model accurately predicted the behavior of a strongly finite-rate driven lean flame at $\varphi = 0.43$, with the assumptions used in the Eddy Dissipation Concept (EDC) proving more effective in the highly turbulent shear layer. The over-prediction observed is linked to the EDC strategy for reaction rate closure at low Reynolds numbers.

Our findings demonstrate that controlling the equivalence ratio around 1 maximizes combustion temperature, which aligns with theoretical and experimental findings. Variations in the equivalence ratio can reduce the temperature, as increasing air reduces heat release and decreasing air leads to incomplete combustion. Preheating the air can further increase combustion temperature.

OpenFOAM has proven to be an effective tool for studying turbulent combustion in computational fluid dynamics (CFD). Its open-source nature and flexibility make it invaluable for researchers. However, studying the complexity of combustion requires more precise turbulence models like LES to accurately capture flow dynamics and combustion processes.

Given the limitations of the realizable k-epsilon model and the need for high-fidelity simulations, it is crucial to continue working on this subject. Further research and development are necessary to enhance the accuracy of turbulence models and gain a better understanding of interactions within turbulent combustion. This ongoing work is essential for improving predictive capabilities and developing more efficient and cleaner combustion systems.

Highlights:

- Equivalence Ratio Impact: The model demonstrated better agreement with experimental flame lengths for φ = 0.43 compared to φ = 0.56, indicating its suitability for scenarios with finite rate dominance.
- Temperature Control: Controlling the equivalence ratio around 1 maximizes combustion temperature, while variations can either decrease temperature (due to excess air) or result in incomplete combustion (due to insufficient air).
- Preheating Effect: Preheating the air mixture to 673 K increases the combustion temperature.
- Model Limitations: The realizable k-epsilon model exhibits limitations in regions with sudden changes in section area, leading to non-physical turbulent viscosities and inaccuracies in turbulent velocity profiles.
- Turbulence Modeling: Complex anisotropic interactions in shear-layer turbulence suggest the need for a scale-resolving approach like LES to capture flow physics more accurately.
- Tool Effectiveness: OpenFOAM's flexibility and open-source nature make it a valuable CFD tool for studying turbulent combustion. However, more precise turbulence models are necessary for complex combustion dynamics.

Outlook

Based on the findings of this study, several promising avenues for future research and development are identified:

1. **Advanced Turbulence Models**: Implementing and testing more advanced turbulence models, such as Large Eddy Simulation (LES), to improve the accuracy of flow simulations.
2. **Expanded Chemical Mechanisms**: Including additional species and reactions in the chemical mechanisms to enhance the understanding of combustion processes.
3. **Multi-Physics Integration**: Coupling CFD with detailed heat transfer and radiation models to provide a comprehensive understanding of turbulent combustion interactions.

References:

1. [Online] https://spinoff.nasa.gov/node/9296.
2. **Tennekes, H., Lumley, J.L.** *A first course in turbulence.* s.l. : MIT Press, 1997.
3. **Warnatz, J., Maas, U., Dibble, R.W.** *Combustion.* s.l. : Springer Verlag, 1996.
4. [Online] https://help.sim-flow.com/solvers/reacting-foam.
5. **Khush Bakhat Rana, Boštjan Mavrič, Rizwan Zahoor, Bozidar Sarler.** *A meshless solution of the compressible viscous flow in axisymmetric tubes with varying cross-sections.*
6. **https://www.cfd-online.com/Wiki/Continuity_equation.** [Online]
7. **CHUNG, T. J.** *COMPUTATIONAL FLUID DYNAMICS.* second Edition.
8. [Online] https://help.altair.com/hwcfdsolvers/acusolve/topics/acusolve/training_manual/realizable_k_e_model_r.htm.
9. [Online] https://doc.cfd.direct/openfoam/user-guide-v6/thermophysical.
10. **Qi Yanga, Peng Zhao, Haiwen Ge.** *reactingFoam-SCI: An open source CFD platform for reacting flow.* a Department of Mechanical Engineering, Oakland University, Rochester, MI 48309, USA; Department of Mechanical Engineering, Texas Tech University, Lubbock, TX 79409, USA : s.n., 2019.
11. **William H. Press, Saul A. Teukolsky, William T. Vetterling, Brian P. Flannery.** *NUMERICAL RECIPES The Art of Scientific Computing.* Cambridge University : 17.5.1 Rosenbrock Methods, 2007.
12. **012026, D C Toncu et al 2015 IOP Conf. Ser.: Mater. Sci. Eng. 95.** On methane pyrolysis special applications.
13. **POPE, B. YANG* and S. B.** *An Investigation of the Accuracy of Manifold Methods and.* New York 14853-7501.
14. [Online] https://www.afs.enea.it/project/neptunius/docs/fluent/html/th/node112.htm.
15. [Online] https://www.tfd.chalmers.se/~hani/kurser/OS_CFD_2009/AlexeyVdovin/Radiation_in_OpenFoam_final.pdf.
16. **Jella, Sandeep E.** *CFD MODELING OF EQUIVALENCE RATIO EFFECTS ON A PRESSURIZED TURBULENT PREMIXED FLAME.*
17. [Online] https://www.idealsimulations.com/resources/turbulence-models-in-cfd/.
18. **Inc, Fluent.** *Modeling Turbulence.* septemper 29, 06.
19. **Siewert, Piotr.** *Flame front characteristics of turbulent lean premixed methane / air flames at high-pressure.*
20. **Guangpeng Li, Hengchao Zhou and Qi Wang.** *Experimental Study on the Influence of Preheated Air and Air-fuel Ratio on the Combustion.*
21. **Helen H. Lou, *,† Daniel Chen,† Christopher B. Martin,‡ Xianchang Li,§ Kuyen Li,† Hitesh Vaid,†.** *Optimal Reduction of the C1−C3 Combustion Mechanism for the simulation of Flaring.*
22. [Online] https://doc.cfd.direct/openfoam/user-guide-v6/thermophysical.
23. [Online] https://en.wikipedia.org/wiki/Rosenbrock_function.

24. **Bilger, R.W., Pope, S.B., Bray, K.N.C., Driscoll, J.F.** *Paradigms in Turbulent.* 2005. Proceedings of the Combustion Institute, 2005. 30: p. 21-42. .
25. **J. G. VERWERt, E. J. SPEEt, J. G. BLOMt, AND W. HUNDSDORFERt.** *A SECOND-ORDER ROSENBROCK METHOD APPLIED TO PHOTOCHEMICAL DISPERSION PROBLEMS**. © 1999 Society for Industrial and Applied Mathematics : SIAM J. SC!. COMPUT. Vol. 20, No. 4, pp. 1456··1480.

APPENDIX

This includes most of the files used for the simulations; each simulation will be a modification of the values put on this case

.

The rest of the Files not mentioned here are the same of the “sandia D Flame” tutorial case. The gas thermodynamic proprieties are directly taken from chemkinToFoam command from the original chemkin files available online.

system/controlDict

```
FoamFile
{
   version        2;
   format         ascii;
   class          dictionary;
   object         controlDict;
}

application     reactingFoam;

startFrom       latestTime;

startTime       0;

stopAt          nextWrite;//endTime;//

endTime         0.074;//0.297;

deltaT          1e-5;

writeControl    runTime;//timeStep;

writeInterval   0.000004;//1

purgeWrite      0;

writeFormat     binary;

writePrecision  10;

writeCompression off;

timeFormat      general;

timePrecision   6;

runTimeModifiable true;
adjustTimeStep    yes;
maxCo           0.65;
maxDeltaT       1e-4;

functions
{
   }
```

system/fvSchemes

```
FoamFile
{
    version     2.0;
    format      ascii;
    class       dictionary;
    object      fvSchemes;
}
// * * * * * * * * * * * * * * * * * * * * * * * * * * * * * * * * * * * * * * * * * * * * //
ddtSchemes
{
    default         Euler;
}

gradSchemes
{
    default         Gauss linear;
}

divSchemes
{
    default           none;

    div(phi,U)          Gauss limitedLinearV 1;

    div(phi,Yi)         Gauss limitedLinear01 1;
    div(phi,h)          Gauss limitedLinear 1;
    div(phi,K)          Gauss limitedLinear 1;
    div(phid,p)         Gauss limitedLinear 1;
    div(phi,epsilon)    Gauss limitedLinear 1;
    div(phi,Yi_h)       Gauss limitedLinear01 1;
    div(phi,k)          Gauss limitedLinear 1;
    div(((rho*nuEff)*dev2(T(grad(U)))))     Gauss linear;
}

laplacianSchemes
{
    default         Gauss linear orthogonal;
}

interpolationSchemes
{
    default         linear;
}

snGradSchemes
{
    default         orthogonal;
}
```

system / fvSolution

```
FoamFile
{
   version     2.0;
   format      ascii;
   class       dictionary;
   object      fvSolution;
}
solvers
{
   "rho.*"
   {
      solver          diagonal;
   }

   p
   {
      solver           PCG;
      preconditioner   DIC;
      tolerance        1e-7;
      relTol           0.1;
}
   ppyFoamPlotWatcher.py
   {
      solver          PCG;
      preconditioner  DIC;
      tolerance       1e-3;
      relTol          1;
   }

   pFinal
   {
      $p;
      relTol          0;
   }

   "(U|h|k|epsilon)"
   {
      solver          PBiCGStab;
      preconditioner  DILU;
      tolerance       1e-7;
      relTol          0.05;
   }

   "(U|h|k|epsilon)Final"
   {
      $U;
   }
```

```
    Yi
    {
        solver          PBiCGStab;
        preconditioner  DILU;
        tolerance       1e-7;
        relTol          0.05;
    }

    G
    {
        solver          PCG;
        preconditioner  DIC;
        tolerance       1e-5;
        relTol          0.1;
    }

    GFinal
    {
        $G;
        relTol          0;
    }
}

PIMPLE
{
    momentumPredictor   yes;
    nOuterCorrectors    1;
    nCorrectors         3;
    nNonOrthogonalCorrectors 0;
    maxDeltaT           1e-4;
    maxCo               0.9;//0.15;
    alphaTemp           0.05;
    alphaY              0.05;
    Yref
    {
        O2              0.1;
        CH4             0.1;
    }
    rDeltaTSmoothingCoeff   0.025;
    rDeltaTDampingCoeff     1;

}

relaxationFactors
{
    equations
    {
        ".*"            0.9;
    }
}
```

system / setFields

```
FoamFile
{
    version     2.0;
    format      ascii;
    class       dictionary;
    object      setFieldsDict;
}
// * * * * * * * * * * * * * * * * * * * * * * * * * * * * * * * * * * * * * * * * * * * * //



regions
(
    boxToCell
    {

        box (0.000 0.0345 -1) (0.003 0.0375 0);
        fieldValues
        (
            volScalarFieldValue T 3000       );

    }
);
```

system / blockMeshDict

```
FoamFile
{
    version     2.0;
    format      ascii;
    class       dictionary;
    object      blockMeshDict;
}
// * * * * * * * * * * * * * * * * * * * * * * * * * * * * * * * * * * * * * * * * * * * * //

mergeType topology;//points;   // Wedge geometry - Merge points instead of topology

scale   0.001;

vertices
(
    (-30 0 0) //0
    (0 0 0) //1
    (0 12.5 0) //2
    (-30 12.5 0) //3
    (320 0 0) //4
    (320 37.5 0) //5
    (0 37.5 0) //6
    (350 0 0) //7
    (350 32.5 0)//8
    (400 0 0)//9
    (400 32.5 0)//10
    (-30 0 -1000) //11
    (0 0 -1000) //12
    (0 12.5 -1000) //13
    (-30 12.5 -1000) //14
    (320 0 -1000) //15
    (320 37.5 -1000) //16
    (0 37.5 -1000) //17
    (350 0 -1000) //18
    (350 32.5 -1000)//19
    (400 0 -1000)//20
    (400 32.5 -1000)//21


);

blocks
(
    hex ( 1 0 3 2 12 11 14 13)   (30  32 1)   simpleGrading (1 1 1)
    hex ( 4 1 6 5 15 12 17 16)   (320  32 1)   simpleGrading (1 1 1)

    hex ( 7 4 5 8 18 15 16 19)   (30  32 1)   simpleGrading (1 1 1)
```

```
    hex ( 9 7 8 10 20 18 19 21)   (50  32 1)   simpleGrading (1 1 1)
);

boundary
(
    inlet
    {
        type patch;
        faces
        (
            (0 3 14 11)
            (6 2 13 17)
        );
    }

    wall
    {
        type wall;
        faces
        (
            (14 3 2 13)
            (13 2 6 17)
            (6 5 16 17)
            (19 16 5 8)
            (8 10 21 19)
        );
    }


    outlet
    {
        type patch;
        faces
        (
            (20 21 10 9)

        );
    }

    symmetry
    {
        type symmetry;
        faces
        (
            (1 12 15 4)
            (0 11 12 1)
            (4 15 18 7)
            (7 18 20 9)

        );
```

```
    }

    frontAndBack
    {
        type empty;
        faces
        (
            (0 1 2 3)
            (1 4 5 6)

            (4 7 8 5)
            (7 9 10 8)
            (14 13 12 11)
            (12 17 16 15)
            (16 19 18 15)
            (18 19 21 20)
        );
    }

);
```

constants / chemistryProprities

```
FoamFile
{
    version         2;
    format          ascii;
    class           dictionary;
    object          chemistryProperties;
}

chemistryType
{
    solver          EulerImplicit;//ode;
    method          TDAC;
}

chemistry       on;

importantSpecies
{
    CO2             ;
    H2O             ;
    CH4             ;
    O2              ;
}

initialChemicalTimeStep 1e-07;

EulerImplicitCoeffs
{
cTauChem 1;
equilibriumRateLimiter off;
```

```
}


odeCoeffs
{
    solver          seulex;
    absTol          1e-9;
    relTol          1e-04;
}
```

constant / combustionProprities

```
FoamFile
{
    version     2.0;
    format      ascii;
    class       dictionary;
    object      combustionProperties;
}
combustionModel  EDC;

active  true;

EDCCoeffs
{
    version v2005;
}
```

constant / turbulenceProprities

```
FoamFile
{
   version     2.0;
   format      ascii;
   class       dictionary;
   object      turbulenceProperties;
}
// * * * * * * * * * * * * * * * * * * * * * * * * * * * * * * * * * * * * * * * * * * * * //

simulationType      RAS; //RAS;

RAS
{
   RASModel        realizableKE;


   turbulence      on;

   printCoeffs     on;

   realizableKECoeffs
   {
      A0          2;
      C2          1.9;
      sigmak      1;
      sigmaEps    1.2;
   }
}
```

constant / boundaryRadiationProperties

```
FoamFile
{
    version     2.0;
    format      ascii;
    class       dictionary;
    object      boundaryRadiationProperties;
}
// * * * * * * * * * * * * * * * * * * * * * * * * * * * * * * * * * * * * * * * * * * * * //

".*"
{
    type            lookup;
    emissivity      1;
    absorptivity    0;
}
```

0 / P

```
FoamFile
{
   version     2.0;
   format      ascii;
   class       volScalarField;
   object      p;
}

dimensions      [1 -1 -2 0 0 0 0];

internalField   uniform 500000;

boundaryField {

symmetry
   {
      type          symmetry;
   }

   frontAndBack
   {
      type          empty;
   }

   wall
   {
      type          zeroGradient;

}

   outlet
```

```
    {
        type            waveTransmissive;
        psi             thermo:psi;
        lInf            1;
        field           p;
        gamma           1.4;
        fieldInf        500000;
        value           $internalField;

    }
    inlet
    {

        type            zeroGradient;
    }

}
```

0/T

```
FoamFile
{
    version     2.0;
    format      ascii;
    class       volScalarField;
    object      T;
}
// * * * * * * * * * * * * * * * * * * * * * * * * * * * * * * * * * * * * * * * * * * * * //

dimensions      [0 0 0 1 0 0 0];

internalField   uniform 800;

boundaryField {    symmetry
    {
        type            symmetry;
    }

    frontAndBack
    {
        type            empty;
    }

    inlet
    {
        type            fixedValue;
        value           uniform 800;

}

    wall
```

```
    {
        type            zeroGradient;
    }

    outlet
    {
        type            zeroGradient;
    }

}
```

0 / U

```
FoamFile
{
    version     2.0;
    format      ascii;
    class       volVectorField;
    object      U;
}
// * * * * * * * * * * * * * * * * * * * * * * * * * * * * * * * * * * * * * * * * * * * * //

dimensions      [0 1 -1 0 0 0 0];

internalField   uniform (0 0 0);

boundaryField {    symmetry
    {
        type            symmetry;
    }

    frontAndBack
    {
        type            empty;
    }

    wall
    {
        type            noSlip;

}
```

```
    outlet
    {
        type            zeroGradient;
    }


    inlet
    {
        type            fixedValue;
        value           uniform (40 0 0);
    }

}
```

0 / k

```
FoamFile
{
    version     2.0;
    format      ascii;
    class       volScalarField;
    object      k;
}
// * * * * * * * * * * * * * * * * * * * * * * * * * * * * * * * * * * * * * * * * * * * * //

dimensions      [0 2 -2 0 0 0 0];

internalField   uniform 110;

boundaryField {    symmetry
    {
        type            symmetry;
    }

    frontAndBack
    {
        type            empty;
    }

    wall
    {
        type            kqRWallFunction;
        value           $internalField;

}

    outlet
    {
```

```
        type            zeroGradient;
    }



    inlet
    {
        type            fixedValue;
        value           uniform 110;

}
}
```

0 / epsilon

```
FoamFile
{
    version     2.0;
    format      ascii;
    class       volScalarField;
    object      epsilon;
}
// * * * * * * * * * * * * * * * * * * * * * * * * * * * * * * * * * * * * * * * * * * * * //

dimensions      [0 2 -3 0 0 0 0];

internalField   uniform 104433;

boundaryField {    symmetry
    {
        type            symmetry;
    }

    frontAndBack
    {
        type            empty;
    }

    wall
    {
        type            epsilonWallFunction;

        value           uniform 104433;

}
```

```
    outlet
    {
        type            zeroGradient;
    }


inlet
{
    type            fixedValue;
    value           uniform 104433;
        }

}
```

0 / CH4

```
FoamFile
{
    version     2.0;
    format      ascii;
    class       volScalarField;
    object      CH4;
}
// * * * * * * * * * * * * * * * * * * * * * * * * * * * * * * * * * * * * * * * * * * * * //

dimensions      [0 0 0 0 0 0 0];

internalField   uniform 0.031603;

boundaryField {    symmetry
    {
        type            symmetry;
    }

    frontAndBack
    {
        type            empty;
    }

    inlet
    {
        type            fixedValue;
        value           uniform 0.031603;

}

    wall
```

```
    {
        type            zeroGradient;
    }


    outlet
    {
        type            zeroGradient;
    }
}
```

All other species have the same initial and boundary conditions but the values differ.